Dissertation for the Degree of

Master of Landscape Architecture

The effect of building form and sky view factor on daytime land surface temperature in residential street canyons, Seoul, Korea

서울시 주거지역 옥외공간의 건축형태와
천공률에 따른 주간 표면온도 영향 분석

August 2016

Graduate School of Seoul National University

Department of Landscape Architecture

Jun Sik Kim

The effect of building form and sky view factor on daytime land surface temperature in residential street canyons, Seoul, Korea

지도교수 이 동 근

이 논문을 조경학 석사 학위논문으로 제출함

2016 년 **4** 월

서울대학교 대학원

조경지역시스템공학부 생태조경학 전공

김 준 식

김준식의 석사 학위논문을 인준함

2016 년 **6** 월

위 원 장 _____ (인)

부위원장 _____ (인)

위 원 _____ (인)

■ Abstract

The effect of building form and sky view factor on daytime land surface temperature in residential street canyons, Seoul, Korea

Advisor Prof. : Dong-Kun Lee
Seoul National University
Department of Landscape Architecture
Junsik Kim

Urbanization causes significant urban climate change, especially with increasing temperatures. This is called the 'Urban Heat Island (UHI)' effect and affects human health and the quality of life. Changes in urban geometry are one of the key factors causing the UHI. Building structures change the urban canyon form that, in turn, changes the thermal condition in the urban canyon. Therefore, a quantitative analysis of the effect of building structures on the thermal conditions in an urban canyon is very important for urban planning.

A commonly used indicator to describe the urban geometry is the sky view factor (SVF). This indicator, often denoted by Ψ_{sky}, indicates the ratio of the radiation received (or emitted) by a planar surface from the sky to the radiation emitted (or received)

from the entire hemispheric radiating environment. With its important role in radiation balance schemes, the SVF has been widely used by climatologists to investigate the relationships between urban geometry and thermal conditions.

Many previous studies using photographic methods use a fish-eye lens to take onsite photographs that project the hemispheric environment onto a circular plane. However, this method is limited as direct sunlight or different cloud types can cause problems in image processing. The photographic method is used to extract some points by taking a picture at specific points. However, some points do not represent the correct values for the site, as SVF can have different values in the same urban canyon because of the distance from the buildings. Because of these limitations, software methods have been developed as computer performance has rapidly increased and digital mapping techniques have become prominent. Recently, software methods have been frequently used in the analysis of the urban thermal condition. The software methods increase processing speeds, while the accuracy of the method depends on the resolution of the raster database in the digital elevation model (DEM). For high accuracy, there needs to be high resolution images of the buildings and a topography database. These methods offer rapid ways of calculating the continuous SVF for large areas based on comprehensive analyses, and studies using this method have increased recently.

The collection of temperature data in previous studies has relied

on onsite surveys using thermometers to understand the thermal condition. However, since the microclimate has complex characteristics and is affected by many factors, the collection of representative temperatures is challenging in limited sample sites. Therefore, land surface temperatures (LST) obtained by remote sensing, which has been used by many previous studies, has advantages for analyzing the relative thermal condition in large areas simultaneously.

With these advantages, some recent studies have analyzed the correlation between the simulated SVF and LST for understanding the thermal condition. However, there are limitations. First, the LST and the temperature pattern characteristic by land use are not controlled and can be very different. Second, since Landsat 8 has a 30 m LST resolution, the measurement of the thermal condition of building outdoor space and the effect of the surface temperature controlled by the roof (building) coverage ratio need to be considered. This is also missing. Third, the distance to a thermal reduction component is an important factor, because mountains, rivers, and green space have a cooling effect. In addition, different types of land cover have unique thermal characteristics. These factors have been disregarded in previous studies. The building arrangement effect on the thermal condition has also been disregarded. Both of these effects are included in this study.

The goal of this study is to develop a quantitative measurement for the relationship among building forms, the shape of the urban

canyon, and the thermal condition in the urban canyon using a suitable method for large areas considering the limitations of previous studies. Therefore, this study analyzes the correlation among LST obtined by remote sensing, SVF obtained by SVF simulation and building heights by roof (building) coverage ratio group. I analyzed results the mechanisms in previous studies and the green space in residential areas using the normalized difference vegetation index (NDVI) especially for the study site, which is a residential area where there is land use control. I especially focused on residential areas, since the thermal comfort of residential areas directly effects vulnerable people, such as children and the elderly.

In this analysis, I attempted to evaluate the components directly affecting thermal reduction, such as mountains, the Hangang River, streams, and green space. In addition, there were efforts to find an organic relationship among building height, the SVF in outdoor space, and the LST by each similar roof (building) coverage ratio group to control the problem. Because there is a limitation in the study caused by LST resolution.

To sum up the results of this study, first, low rise buildings, such as detached houses and multi-family housing, result in a high SVF condition, which can be explained by the formation of an urban canyon. A high SVF results in a high LST caused by the increased net radiation near the ground because of increased direct solar radiation. In contrast, high-rise buildings, such as

apartments or tower type apartments, result in low SVF in the urban canyon and a low LST environment.

Second, there are sections with different SVF values even with similar heights for high rise building, caused by the arrangement of the high rise flat-type apartments. The extracted area with an SVF value under 0.2 in the simulated data is an enclosed type arrangement with shapes such as a 'C' or 'O'. An open type arrangement with an 'L' or 'I' shape has SVF values mostly over 0.2. As the SVF decreases, the LST increases in the zone with SVF values under 0.2, such as in the enclosed arrangements. The enclosed arrangement form of a flat-type apartment has a high LST, and these areas have a poor radiant cooling ability at night caused by the low SVF. Therefore, enclosed type high rise buildings should be avoided in urban planning.

This pattern with an SVF under 0.2 is unique. Therefore, I focused on this section and to develop the reasons for these results. The first hypothesis is based on previous studies. An area with a small SVF value leads to a decline in long wave radiation, resulting in increasing counter radiation in the nighttime. Therefore, the limited cooling of the surface in the nighttime influenced the daytime surface. The Landsat 8 LST on site is 11 a.m. At this time, the sun's elevation is not high enough to heat the surface in the low SVF area. Therefore, there is not enough direct solar radiation on the surface and the nighttime pattern still is present in the daytime in the area with the SVF under 0.2.

The second hypothesis is that the area with the SVF value under 0.2 has lower green space than the area with SVF over 0.2. In a previous study, Moon (2011) found a pattern showing that the courtyard of enclosed arrangement flat-type apartments has more parking lot and lower green space than the other types. Therefore, the analysis between NDVI and SVF focused on the area with the SVF value under 0.2. The results show that NDVI and SVF have a positive relationship at all SVF values. In sections with the SVF under 0.2, the NDVI ratio increase ratio is higher than in the other sections. In sections with the SVF under 0.2, as SVF increased, NDVI increased while LST decreased, indicating NDVI affects the decrease in LST. In contrast, in sections with SVF values over 0.2, as SVF increased, NDVI increased, and LST increased. This pattern means the mechanism of increasing direct solar radiation is affected by an increase in NDVI.

The goal of this study is to find quantitative correlations among building forms, the urban canyon, and the thermal environment using simulated SVF based on high resolution data and remote sensing. This study can use the basic data from urban planning or building architecture. Ultimately, this study can contribute to sustainable development.

❑ *Keywords : Sky view factor(SVF), Land surface temperature(LST), Building height, Residential area, Urban heat island*

❑ *Student Number : 2014-22917*

Table of contents

List of figures

List of tables

1. Introduction

Urbanization causes significant urban climate change, especially increasing temperatures. This phenomenon is called the 'Urban Heat Island (UHI)' effect. Recently, climate change has accelerated the UHI effect. A UHI is a city or metropolitan area that is significantly warmer than its surrounding rural areas due to human activities, such as population growth, artificial heating, changes in land cover, and increases in vehicles (Landsberg, 1981). The UHI effect leads to negative effects on human health and the quality of life (Baker et al., 2002; Patz et al., 2005). Therefore, monitoring the thermal environment in urban areas is of increasing importance. Recently, many studies have focused on the thermal environmental, such as the thermal patterns in urban area and the characteristics of vulnerable areas.

The change in urban geometry is a key factor causing the UHI. Building structures change the urban canyon form that, in turn, changes the thermal condition in the urban canyon. Previous studies have found that a lower sky view factor (SVF) is one of the main factors generating the UHI according to a high density, high rise build up (Voogt and Oke, 1997; WMO, 2006). Therefore, a quantitative analysis of the effect of building structures on the thermal condition in the urban canyon is very important in terms of urban

planning.

A commonly used indicator to describe the urban geometry is the SVF. This indicator, often denoted by Ψ_{sky}, indicates the ratio of the radiation received (or emitted) by a planar surface from the sky to the radiation emitted (or received) from the entire hemispheric radiating environment (Watson and Johnson, 1987). In other words, the SVF includes the three-dimensional (3-D) urban canyon form and the radiation ratio on the surface.

The SVF changes from day to night to affect the thermal environment. In the daytime, the SVF values are decreased by high rise, high density buildings. It leads to a decrease in the direct solar radiation on surfaces, the surface heat fluxes, surface temperatures, mean wind speeds, and turbulent kinetic energy. It results in decreasing air temperature. However, in the nighttime, the thermal turbulence and surface heat flux increase and the cooling effect decreases. This is because the outgoing long wave radiation is decreased by obstacles. This thermal pattern increases net radiation and counter radiation in the urban canyon. The net radiation and counter radiation are absorbed in the ground surface or the surface of buildings, increasing urban heat (He et al., 2013; Chen., 2012; Voogt, 2010; Svensson, 2004).

Several authors have shown a statistically significant

relationship between surface temperature and the SVF. This result is expected since the energy balance of the surface affects the surface temperature (Svensson, 2004; Barring et al., 1985; Eliasson, 1996; Upmanis, 1999; Postgard, 2000; Chapman et al., 2001).

However, Korea did not consider the SVF in urban planning or building law. This is because there is an unclear of relationship between building forms and the outdoor thermal environment. Therefore, there is a need to understand the thermal environment quantitative effects by defining these relationships.

A residential area's thermal environment is more important than other land use types because the thermal condition affects directly the life of residents and vulnerable people, such as children and the elderly. There are different characteristic thermal patterns for each type of land use. Therefore, land use control is necessary in the understanding of thermal patterns based on building structures (Svensson, 2004).

The location is important in order to find pure relationships between building structures and the thermal condition, including the distance to thermal reduction components. Mountains, rivers, and green space have a powerful cooling effect, especially in Seoul, which has big mountains and a broad river, greatly affecting temperature. Therefore, the

distance from these thermal reduction components must be regarded as a cooling range.

In previous studies, the temperature values were taken onsite using thermometers to understand the thermal condition. However, a microclimate has complex characteristics and is affected by many factors. Therefore, acquiring representative temperature values is very hard in limited sample sites. Therefore, it is useful to use the land surface temperature (LST) obtained by remote sensing. This can analyze large areas while acquiring data to understand the relative thermal condition. Many previous studies using LST promoted these advantages. However, the LST scale is larger than other methods, so the roof ratio is must be regarded for the measurement of the outdoor thermal environment.

The SVF is a useful and effective way of representing the 3-D form of the outdoor space. Many previous studies used the SVF with photographic methods for specific sites. However, it is not suitable for large area measurements because some points are not represented in a large area. In addition, one of the characteristics of SVF is having different values in the same urban canyon depending on the distance from the measuring point to a building. Therefore, there is a need to find a suitable method of determining a quantitative relationship between SVF and surface temperature in large

areas.

For these reasons, the goal of this study is to develop a quantitative measurement for the relationship among building forms, the shape of the urban canyon, and the thermal condition in the urban canyon using a suitable method for large areas. Therefore, this study analyzes the correlation among LST obtained by remote sensing, SVF obtained by SVF simulation and building heights using latest high resolution building data by roof (building) coverage ratio group. To further evaluate the results, the mechanisms in previous studies were analyzed and the green space in residential area was evaluated using the normalized difference vegetation index (NDVI).

This is important in the study site, a residential area, which must consider land use control. The direct effect of thermal reduction components, such as the mountains, the Hangang River, streams, and green space, was also evaluated. Areas with similar roof (building) coverage ratios were compared to find organic relationships among building height, the SVF in outdoor spaces, and LST. This was done to control the LST resolution problems.

The first hypothesis of this study was that low rise buildings, such as detached houses and multi-family housing, lead to high SVF values. The high SVF leads to high LST caused by increases in net radiation near the ground because

of increased direct solar radiation. In contrast, high-rise buildings, such as flat-type apartments or tower type apartments, lead to low SVF in urban canyons, which leads to a low LST. The second hypothesis states that there are zones of different SVF values even if there are similar building heights in the high rise building sector. An enclosed arrangement of high rise flat-type apartments has a lower SVF than an open type arrangement. A third hypothesis suggests that there are inflection points in the relationship between SVF and LST. There are two reasons for this. First, there is not enough sun elevation to heat surfaces in extremely low SVF sections. Second, the thermal pattern in the nighttime increases net radiation, while counter radiation is absorbed in the ground surface or the building surface in lower SVF sections.

2. Literature review

2.1. Causes of the urban heat island (UHI)

The causes of the UHI can be classified on a meteorological scale with the Urban Boundary Layer (mesoscale) and Urban Canopy Layer (microscale). The causes of urban heat in the Urban Boundary Layer are the slow winds over rough urban surfaces, the addition of heat from roofs and the tops of urban street canyons, pollution of the urban boundary layer, and anthropogenic heat from chimneys and vents. Heat levels in the Urban Canopy Layer are caused by the absorption of solar radiation by low reflectance surfaces and trapping by reflections, impermeable surfaces that reduce surface moisture and evapotranspiration, insulated surfaces leading to high daytime surface temperatures, obstructed views of the sky that trap radiative heat by surfaces, the addition of anthropogenic heat by pollutants and humidity, irrigation of select surfaces, slow winds and increasing turbulence, increased stored heat by the thermal properties of urban materials, and increasing surface area (Stewart and Oke, 1997; WMO, 2006; Voogt, 2007) (Figure 1 and Table 1).

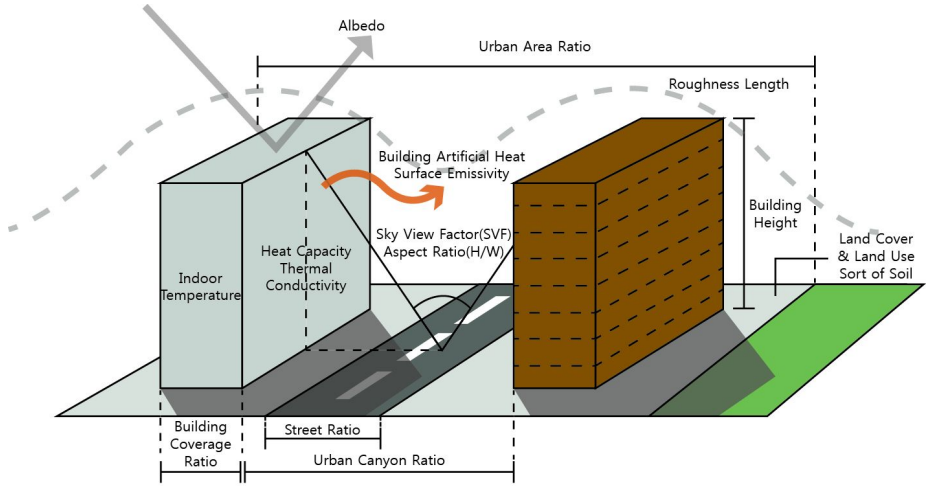

Figure 1. Diagram of thermal increasing components (Source: Junsik Kim)

Table 1. Sort of thermal increasing components

Large Categorize	Medium Categorize	Small Categorize	Reference
Building Construction	Building Geometry	Sky View Factor (SVF)	Wang and Akbari(2014), Oke(2012), Grimmond(2010), Svensson(2004), IA Yeo(2011),
		Aspect Ratio (H/W)	Masson(1999), Masson(2002), Adolphe(2001), Mcpherson(1994), Oke(2012), A. LEMONSU(2004), Nunez and Oke (1977), YH Ryu(2012), SH Lee(2011), IA Yeo(2011),
		Building Height / number of stories	Masson(2002), Kusaka(2004), A. LEMONSU(2004), Kusaka(2001), Adolphe(2001), Nunez and Oke (1977), BR Lee(2015), YH Ryu(2012), SH Lee(2011), IA Yeo(2011),
		Building Width	Landsberg(1981), JJ Lee(2009)
	Building Density	Number of Building	Tokyo Metropolitan Gov.(2005)
		Building Coverage Ratio	Oke(2012), Gago(2013), Mcpherson(1994), IA Yeo(2011)
		Floor area ratio	IA Yeo(2011)
		Roof(building) Ratio	A. LEMONSU(2004), YH Ryu(2012), SH Lee(2011), Kusaka(2004), Kusaka(2001), BR Lee(2015), IA Yeo(2011)
		Urban Canyon Ratio	Masson(2002), A. LEMONSU(2004), YH Ryu(2012), SH Lee(2011)
		Street Ratio	A. LEMONSU(2004), YH Ryu(2012), SH Lee(2011), Kusaka(2004), Kusaka(2001), BR Lee(2015)
Land Use and Land Cover (LULC)	Urban Land Use and Land cover fraction	Urban Area Ratio (Residential/Commercial/Industrial/Street)	Masson(1999), A. LEMONSU(2004), Nunez and Oke (1977), BR Lee(2015), YH Ryu(2012)
		Impervious Surface Area Ratio	Oke(2012)

Large Categorize	Medium Categorize	Small Categorize	Reference
Heat Transfer Variable	Heat Capacity	Heat Capacity in Urban	Kusaka(2004)
		Heat Capacity of Roof	Masson(1999), A. LEMONSU(2004), BR Lee(2015), YH Ryu(2012), SH Lee(2011)
		Heat Capacity of Building Wall	Masson(1999), A. LEMONSU(2004), Nunez and Oke (1977), BR Lee(2015), YH Ryu(2012), SH Lee(2011)
		Heat Capacity of Street Material	Masson(1999), A. LEMONSU(2004), BR Lee(2015), YH Ryu(2012), SH Lee(2011)
		Heat Capacity of Surface	Nunez and Oke (1977)
	Thermal Conductivity	Thermal Conductivity of Roof	Nunez and Oke (1977), Masson(1999), Masson(2002), A. LEMONSU(2004), Kusaka(2004), BR Lee(2015), YH Ryu(2012), SH Lee(2011)
		Thermal Conductivity of Building Wall	Masson(1999), Masson(2002), A. LEMONSU(2004), Kusaka(2004), Nunez and Oke (1977), BR Lee(2015), YH Ryu(2012), SH Lee(2011)
		Thermal Conductivity of Street	Nunez and Oke (1977), Masson(1999), Masson(2002), Kusaka(2004), A. LEMONSU(2004), BR Lee(2015), YH Ryu(2012), SH Lee(2011)
Air Dynamics Variables	Roughness length	Roughness length of Urban	Masson(2002), Oke(2012), Adolphe(2001), Kusaka(2004), Kusaka(2001), SH Lee(2011), Oke(2012)
		Roughness length of Roof	Masson(2002), Kusaka(2004), Kusaka(2001), A. LEMONSU(2004), BR Lee(2015), YH Ryu(2012), SH Lee(2011)
		Roughness length of Urban Canyon	Kusaka(2004), Kusaka(2001)
		Roughness length of Building Wall	BR Lee(2015)
		Roughness length of Street	Masson(2002), A. LEMONSU(2004), BR Lee(2015), YH Ryu(2012), SH Lee(2011)
Radiative Transfer Variables	Surface Albedo	Albedo of Surface	Gago(2013), Grimmond(2010), Akbari and Taha(1992), Taleghani(2014), Wang and Akbari(2014), Oke(2012), Akbari(2001)
		Albedo of Roof Surface	Masson(1999), Masson(2002), Kusaka(2004), Kusaka(2001), A. LEMONSU(2004), YH Ryu(2012), SH Lee(2011), BR Lee(2015)
		Albedo of Building Wall	Masson(1999), Masson(2002), Kusaka(2004), Kusaka(2001), A. LEMONSU(2004), BR Lee(2015), YH Ryu(2012)
		Albedo of Street	Masson(1999), Masson(2002), Kusaka(2004), Kusaka(2001), A. LEMONSU(2004), BR Lee(2015), YH Ryu(2012), SH Lee(2011)
	Surface Emissivity	Emissivity of Surface	Tan(2013), Nunez and Oke (1977)
		Emissivity of Roof Surface	Masson(1999), Masson(2002), Kusaka(2004), Kusaka(2001), A. LEMONSU(2004), BR Lee(2015), YH Ryu(2012), SH Lee(2011)
		Emissivity of Building Wall	Masson(1999), Masson(2002), Kusaka(2004), Kusaka(2001), A. LEMONSU(2004), Nunez and Oke (1977), YH Ryu(2012), SH Lee(2011), BR Lee(2015)
		Emissivity of Street	Masson(1999), Masson(2002), Kusaka(2004), Kusaka(2001), A. LEMONSU(2004), YH Ryu(2012), SH Lee(2011), BR Lee(2015)
Indoor Condition	Building Artificial Heat	Artificial Heat	Oke(2012), YH Ryu(2012), BR Lee(2015)
	Indoor Temperature	Indoor Temperature	Masson(2002), A. LEMONSU(2004)
Outdoor Condition	Sort of Soil	Soil Temperature	Masson(2002), A. LEMONSU(2004)

2.2. Land surface temperature (LST)

There are many measurement approaches for the thermal environments in urban areas, such as fixed towers, traversing the area by vehicles or aircraft, radiosonde, remote sensing by aircraft or satellite, and automatic weather systems (Table 2). The land surface temperature (LST) measurement using remote sensing by satellite is useful for measuring large areas. The LST obtained by remote sensing has advantages in that it can analyze large areas at the same time for their relative thermal condition. A time series analysis can also be conducted using multi temporal images, and the stability of the conditions can lead to an effective relative comparison of thermal environments. Many previous studies used the LST because of these advantages (Li et al., 2013; Zhang et al., 2009; Jung et al., 2011).

Table 2. Measurement approaches of thermal environment

Output	Target	Measurements approaches
Air temperature	Urban boundary layer	1. Fixed tower (Flux tower) 2. Traverse (Aircraft) 3. Remote (Sodar)
	Urban canopy layer	4. Fixed screen 5. Traverse (Automobile)
Surface temperature	Surface	6. Remote sensing (Satellite) 7. Aircraft (Thermal scanner) 8. Ground (Infrared light thermal scanner)

2.3. Sky view factor (SVF)

A commonly used indicator to describe the urban geometry is the SVF. It is often denoted by Ψ_{sky}, indicating the ratio of the radiation received (or emitted) by a planar surface from the sky to the radiation emitted (or received) from the entire hemispheric radiating environment (Watson and Johnson, 1987) (Figure 2). With its important role in radiation balances, the SVF has been widely used by climatologists to investigate the relationships between urban geometry and thermal conditions (Lindqvist, 1970; Oke, 1981; Barring et al., 1985; Yamashita et al., 1986; Eliasson, 1991; Upmanis and Chen, 1999; Svensson, 2004; Gal et al., 2009; Unger, 2009). Yang (2015) analyzed the impact of building density and building height on street surface temperatures using numerical models in Hong Kong. In addition, the SVF is used in the components of many studies. For example, Stewart and Oke (2012) constructed a 'Local Climate Zone' for local thermal environment classification using the SVF. Kusaka (2004), Masson (2002), Lee (2011) used the SVF for physical modeling in the 'Urban Canopy Model.'

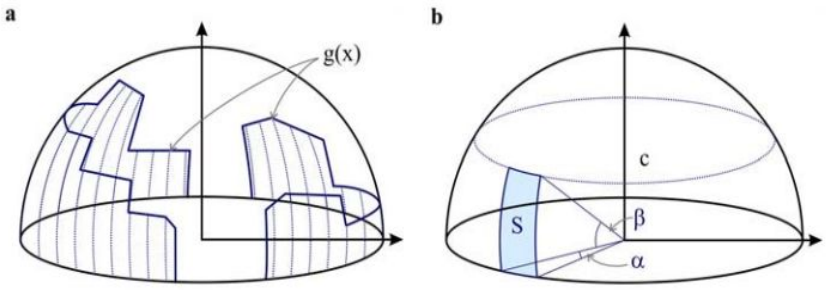

(a) Polygon g(x) as a border of the visible sky and dividing the hemisphere under g(x) equally into slices by angle α

(b) a slice of a 'width' of α (S) of a basin with an elevation angle β

Figure 2. Concept diagram of SVF (Janos Unger, 2009)

Commonly, SVF measurements use four methods; analytical methods, photographic methods, GPS methods, and software methods. Analytical methods are also referred to as geometrical methods. They base the estimation of the SVF on the geometrical characteristics and radiation exchange models of the urban canyons.

Photographic methods have been used in many previous studies. The photographic methods use a fish-eye lens to take onsite photographs that project the hemispheric environment onto a circular plane. The photographs are then processed to define the skyline. The relationship between obstructed and unobstructed parts of the sky is then calculated by appropriate transformations. Photographic methods have been widely used for measurements of SVF from the past to the present. Earlier studies such as Barring

(1985), Eliasson (1996), Upmanis (1999), Postgard (2000), Chapman (2001) focused on the effect of the SVF on air temperature and surface temperature using fish-eye lens photographic methods. They determined the statistical relationship in an urban area. Karlsson (2000) determined the statistical relationship between the SVF and air temperature in urban green areas. Svensson (2004) also focused on the relationship between SVF and air and surface temperature using traverse methods by vehicles. He selected a dense urban canyon because the land use thermal characteristic is big factor. Holmer (2007) analyzed diurnal patterns of cooling rates at different SVF points.

The photographic technique is particularly suitable for determining specific SVFs onsite. It can deal with buildings of various sizes, irregular shapes, and trees. However, this method requires image generation and processing and is often time consuming. In addition, surveying opportunities for this method are limited, as a homogeneous cloudy sky is normally required; direct sunlight or different cloud types will cause problems in image processing (Chapman and Thornes, 2004). Some points in the SVF are not representative of the values for the site. The SVF has different values in the same the urban canyon according to the distance to a building. These limitations make the photographic methods unsuitable for large area analysis (Figure 3).

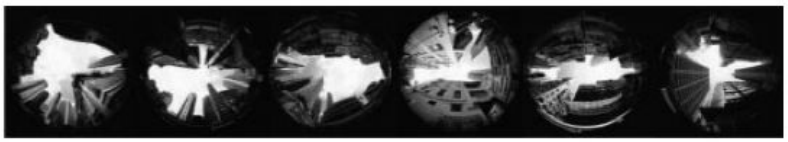

SVF: fish-eye	0.420	0.282	0.410	0.210	0.237	0.204
SVF: simulated	0.442	0.288	0.420	0.258	0.275	0.239

Figure 3. Comparison of SVF between software methods and photographic methods (Chen L et al., 2012)

The GPS methods are based on the direct calculation of the SVF (Chapman et al., 2002). The goal of this method is real time processing using proxy data. A GPS receiver is used to acquire raw data for satellite visibility. The number of visible satellites, the dilution of precision, and the strength of satellite signals were used in a multiple regression analysis to derive a regression equation for the prediction of the SVF. The performance of this method is good only for urban areas.

Software methods use building and topography databases and common GIS-based 3-D models to reconstruct the urban environment in the computer memory. The accuracy of this method depends on the database quality. There are two main approaches for the software methods: vector methods and raster methods.

The vector database simplifies buildings by using flat-roofed blocks represented by polygons. The hemispheric radiating environment is divided equally into slices by a rotation angle. Then, along a particular rotation angle, the

method searches for a single building with the largest elevation angle along that direction. The accuracy of this method depends on the rotation angle and the searching radius. A smaller rotation angle and larger radius result in a more accurate SVF estimation.

The raster-based method is a commonly used way to determine SVF. A digital elevation model (DEM) database is often employed where surface topography and building information are stored in raster format. The software methods need a high resolution building and topography database (Gal et al., 2009). The advantage of a raster-based method is that it is a rapid way to calculate the continuous SVF for large areas. Therefore, raster-based methods have become increasingly recognized in recent studies (Chen et al., 2012).

The SVF simulation approach has continued to develop as computer performance has improved. Ratti and Richens (1999) developed a 'shadow casting' algorithm that calculates building shadow patterns based on a high-resolution DEM. Lindberg (2005) modified an algorithm for calculating SVF, which has been validated. Gal (2006) compared vector methods and raster methods for a correlation analysis with air temperature. Chen (2012) conducted a correlation analysis between raster-based SVF, air temperature, and building volume in a high-density area in Hong Kong (Figure 4). Scarano and Sobrino (2015) analyzed the correlation between raster-based

SVF and LST using remote sensing to overcome a limited number of sample sites in Italy (Figures 5 and 6).

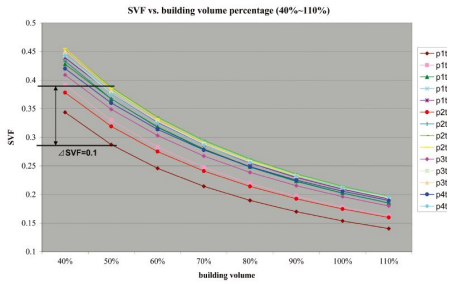

Figure 4. Correlation between building volume and SVF using software methods in Hongkong(Color values: Sites codes) (Chen et al., 2012)

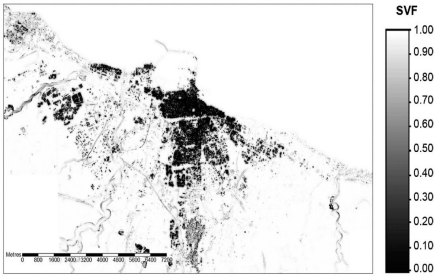

Figure 5. SVF using software methods in Italy, Bari (Scarano and Sobrino, 2015)

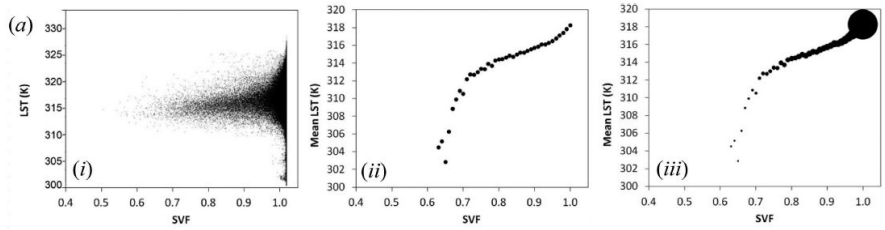

Figure 6. Correlation between simulated SVF and LST using 'Mean analysis'; SVF axis is split into regular intervals of 0.1 units, for each of which the mean value of LST is calculated (Scarano and Sobrino, 2015)

2.4. Literature review conclusion

There are limitations in previous studies dealing with the correlation between the SVF and thermal environment. Many

previous studies used photographic methods with fish-eye lens photos taken onsite for the calculation of the SVF. However, with this method, it is hard to get a representative value of the site because it is influenced by the site condition and the distance from the building in the same urban canyon (Figure 7).

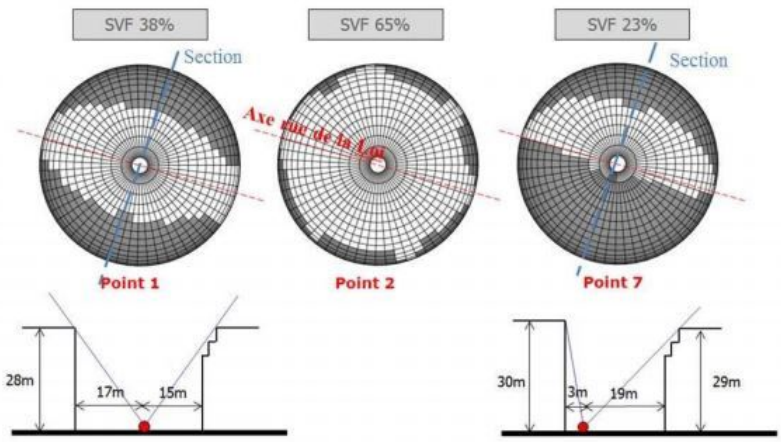

Figure 7. Different values of SVF in same urban canyon according to distance of building (Deroisy B, 2013)

Previous studies have used thermometers for the measurement of temperature in onsite surveys to understanding thermal conditions. However, microclimates have complex characteristics and are affected by many factors. Collecting representative temperature values is challenging with limited sample sites. Therefore, the LST obtained by remote sensing has advantages in the analysis of

relative thermal conditions in large areas. For this reason, the LST has been used in many previous studies.

Therefore, using simulated SVF by raster-based software methods and LST calculated by remote sensing are effective for the measurements in large areas at the same time. With these advantages, Scarano and Sobrino (2015) analyzed the correlation between simulated SVF and LST for understanding the relationship between thermal conditions and city structures.

However, there are limitations. First, the LST temperature pattern characterized by land use was not evaluated. This is significant because the LST thermal characteristic is very different for each land use type (Svensson, 2004). Second, the resampled thermal infrared sensor (TIRS) of Landsat 8 has a 30 m LST resolution. Even when extracting the LST from only building outdoor space, it is affected by the roof cover area because of the LST scale. Therefore, the roof coverage ratio has to be evaluated for measuring the correlation surface temperature and urban canyon. The previous studies did not consider this. Third, the distance from thermal reduction components is an important factor, because mountains, rivers, and green space have a cooling effect. In addition, different types of land cover have unique thermal characteristics, but these factors have not been considered in previous studies. Both of these effects are

evaluated in this study. These factors are important to quantitatively measure the relationship between building structure and the thermal environment.

Therefore, this study considered these areas that limited previous studies. In addition, this study attempted to understand the effect of building arrangement on the thermal condition.

3. Material and methods

3.1. Scope of the study

3.1.1. Temporal scope

For the temporal scope of this study, clear daytime in summer (May-September) for the past three years (2013-2015) was selected to reflect recent urban morphology. The reason for selecting multi temporal periods was to be able to extract representative values in the summer. Daytime in summer was selected because it caused the most trouble for human health, especially for children and the elderly most affected by thermal environments. Five time scenes of fine image quality (Image Quality: 9) with low amounts of cloud on relatively high temperature days were selected (Table 3).

Table 3. Daily meteorological data of selected scenes in Seoul (source: Korea Meteorological Administration)

Time	Average Temperature (℃)	Maximum Temperature (℃)	Minimum Temperature (℃)	Average Cloud Cover	Precipitation (mm)
13/9/16	20.9	27.0	15.2	0.3	-
14/05/30	24.8	31.8	17.3	0.1	-
14/09/19	21.4	28.4	14.9	0.9	-
15/07/04	24.1	29.9	18.2	1.9	-
15/09/22	23.9	31.0	18.0	0.5	-

3.1.2. Spatial scope

Data was obtained in a residential area of Seoul, Korea. This area has high density housing because of a rapidly increasing population. The population of Seoul population was around 10 million in 2016 with a population density of 16 989/km². The highest population density in Seoul is in the borough of Yangcheon-gu at 28 004/km². This density is about the seventh highest in the world, similar to Kamarhati in India (28,696/km²). The increasing population of Seoul has resulted in high density residential development.

Seoul is also known as the 'Republic of the Apartment,' because of the rapidly high density developments to accommodate the population increase. Around 1960, it was common for detached houses and multi-family housing to be built. After that, flat-type apartments were constructed to accommodate the population explosion until 2000. After 2000, the construction of the tower-type apartment building has become typical. These typical forms of residential buildings are densely mixed in Seoul (Table 4 and Figures 8, 9).

Each type of residential building has different typical characteristics for height and arrangement, leading to different urban canyon forms. For this reason, many previous studies focused on the correlation between the residential area form and the thermal environment of the outdoor space in Seoul

(Moon, 2011). The thermal environmental is affected more greatly by urban geometry in a high density city than in a low density city. Therefore, the quantitative analysis of the effects of building structure on the thermal condition in an urban canyon is very important in terms of urban planning. The complex residential building form in the residential areas of Seoul is suitable for the analysis of the building form effect on the thermal condition. Svensson (2004) suggested that different land use has different thermal characteristics. In this study, an area of similar land use was selected for the correlation between building form and thermal environments.

In addition, this study considered the direct cooling effect by thermal reduction components to develop the correct correlation between building forms and the thermal environment. The extracted final site excluded the cooling effect boundary by thermal reduction components such as the rivers, streams, mountains, and green space from previous studies.

Table 4. Present condition of housing in Seoul (Seoul Metropolitan Government, 2015)

	Detached Housing	Multi-family housing	Apartment	Row-House	Others	Total
Number	165,295	1,578,260	1,485,869	145,914	24,435	3,399,773
Percent	4.90%	46.40%	43.70%	4.30%	0.70%	100.00%
Gross Area	Below 330	Below 660	None	Over 660	None	
Floors	Below 3 floor	Below 4 floor	Over 5 floor	Below 4 floor	None	

Figure 8 Residential areas of Seoul (Source: www.yonhapnews.co.kr)

Figure 9 Example of SVF in typical apartment area (Source: Junsik Kim)

3.2. Materials

This study used remote sensing data for the LST. Remote sensing is a tool for collecting data without making physical contact (Liu and Mason, 2009). Optical remote sensing systems measure the solar energy reflected from material surfaces (Reddy, 2008). Landsat 8 (LDCM: Landsat Data Continuity Mission) data provided by the USGS (United States Geological Survey) from May 30, 2013 was used in this study. Landsat 8 is an upgraded version of Landsat 7. The data is collected at 16 day intervals with a 30 m spatial resolution (resampled from 100 m TIRS resolution by USGS).

Landsat 8 carries two instruments. The Operational Land Image (OLI) sensor includes refined heritage bands, along with three new bands: a deep blue band for coastal/aerosol

studies, a shortwave infrared band for cirrus detection, and a quality assessment band. The Thermal Infrared Sensor (TIRS) provides two thermal bands. These sensors both provide improved signal-to-noise (SNR) radiometric performance quantized over a 12-bit dynamic range. The improved SNR performance enables a better characterization of the land cover state and condition. The products are delivered as 16-bit images. The TIRS bands (Band 10 and 11) can vary throughout each scene and depend upon the radiance outside the instrument field of view, which users cannot correct in the Landsat Level 1 data product. Band 11 is significantly more contaminated by stray light than Band 10. Therefore, it is recommended that users refrain from using Band 11 data in quantitative analyses. Landsat 8 Level 1Gt provides systematic, radiometric, and geometric accuracy, while employing a DEM for topographic accuracy (USGS, 2016). Therefore, Landsat 8 Level 1Gt by USGS was selected for this study because it has advantages that provide the stability of data and are suitable for the thermal measurement at city scale (Table 5).

Table 5. Characteristics of 5 scenes satellite data (USGS, 2015)

Time	Cloud Cover (%)	Image Quality	Sun Elevation Angle (°)
13/9/16 11:13 am LTC	0.25	9	51.25
14/05/30 11:10 am LTC	0.16	9	66.72
14/09/19 11:11 am LTC	0.17	9	50.20
15/07/04 11:10 am LTC	6.12	9	66.29
15/09/22 11:11 am LTC	0.35	9	49.14

3.3. Methods

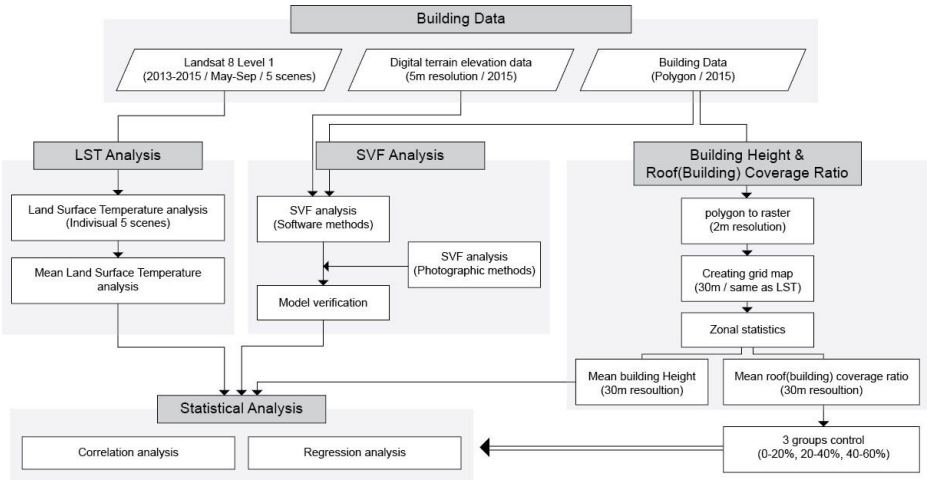

Figure 10. Methods flow chart

The study can be divided into four parts (Figure 10). First, the Landsat 8 LST was constructed across Seoul for the past three years (2013-2015, 5 Scenes) using the Envi 4.1 program. The mean LST was calculated using each LST with the extraction of the final site mean LST. Second, a DEM was constructed using 5 m resolution topography data and 2 m resolution building data. The simulated SVF was calculated using 2 m resolution by the ArcGIS and SagaGIS programs. It was verified by photographic methods. Third, the mean building height and mean roof (building) coverage ratio were calculated using zonal statistics in a 30 m resolution that was

the same as the LST grid. Fourth, statistical analyses, such as correlation analysis and regression analysis, were conducted for building height, SVF, and LST by roof (building) coverage ratio group using SPSS, R, and Tera Plot software.

3.3.1. Site selection

Residential areas were extracted using land use categories in the Seoul biotop map from 2015 provided by the Seoul Metropolitan Government. Outdoor space was selected using the 2015 building data provided by the Ministry of Land, Infrastructure, and Transport. In order to exclude the direct effect from heat reduction components, water components (water surfaces, water edges, and river beds) and green space components (forests, parks, paddies, farms, orchards, planting sites of landscaping trees, botanical gardens, and grassland) were selected by using the land use map (Seoul biotop map). The standard for selecting green spaces is over 10,000 m^2 by area, which is the same as a neighborhood park standard. This is used to remove the range of the direct effect area by the thermal reduction components.

In previous studies, there are general ranges of the affect by thermal reduction components in Korea. A 24 hectare (24,000 m^2) green space provides a cooling effect up to 200-250 m (Lee, 2013). Small and medium sized parks have

an effect up to 120 m (Park, 2014). Water provides a cooling effect up to 200 m (Park, 2010). From these previous studies, a 200 m distance was selected as the direct effect range to be removed using buffer analysis.

3.3.2. Building materials

3.3.2.1. Land surface temperature (LST) analysis

The LST was constructed using band 10 (TIR-1, 10.6-11.19 μm) in Landsat 8 OLI and Envi 4.1 software. The TIRS bands of Landsat 8 are Band 10 and 11, but USGS recommended Band 10 because Band 11 is contaminated by stray light. In a previous study, Xiaolei (2014) compared Band 10 and Band 11 for calculating the LST. The study showed that Band 10 has a value of 1 k under RMSE. This has a better accuracy than using Band 11. The standard Landsat 8 data is provided in the form of Digital Numbers (DN). The first step in calculating LST is the conversion from DN to TOA Radiance. The OLI and TIRS band data can be converted to TOA spectral radiance using the radiance rescaling factors. These are provided in the metadata file.

$$L_\lambda = (M_L * Q_{cal}) + A_L \qquad \text{Equation (1)}$$

L_λ is TOA spectral radiance ($w/m^2/sr/\mu m$). M_L and A_L are Band-specific rescaling factor from the metadata. Q_{cal} is Quantized and calibrated standard product pixel values (DN, 0~32767). The observed radiation temperature of satellites can be calculated using the relationship between absolute temperature (K) and L_λ calculated by equation (1).

$$T(K) = \frac{K_2}{\ln(\frac{K_1}{L_\lambda}+1)} \qquad \text{Equation (2)}$$

$T(K)$ is At-satellite brightness temperature (K) (Equation 2). K_1 and K_2 are Band-specific thermal conversion constants from the metadata (USGS, 2015).

$$T_s = \varepsilon^{-\frac{1}{4}} T(K) \qquad \text{Equation (3)}$$

The land surface temperature (T_s) is calculated by equation (3) using satellite brightness temperature ($T(K)$) and emissivity (ε, Mallick et al.,2008) by land use type. The final site of this study has equal land use, so equal emissivity values are used (ε=0.912, $\varepsilon^{-\frac{1}{4}}$=1.0232). The atmosphere influences the LST. However, if the atmosphere condition is

equal in the entire observation area, no atmosphere correction is needed (Ji et al., 2014). This is verified by the position error in the fives scenes for the LST and the calculated mean LST by ArcGIS software.

3.3.2.2 Sky view factor (SVF) simulation analysis

A commonly used indicator to describe the urban geometry is the SVF. It is calculated as the fraction of sky visible when viewed from the ground up. The SVF is a dimensionless value that ranges from 0 to 1. An SVF value of 1 denotes that the sky is completely visible.

The SVF calculation uses a DEM. The DEM contains the sum of the height of the topography and the height of buildings. The topography height data has a 5m resolution, and it is resampled at a 2m resolution in the ArcGIS software program. The latest polygon building height data by the Ministry of Land, Infrastructure, and Transport in 2015 was used. This polygon data was modified to 2 m resolution raster data to be the same as the topography. The sum of their heights was used in a raster calculator for constructing the final DEM. The SVF was calculated for each 2 m pixel by using Equation (4) using previous DEM data (Bohner and Antonic, 2009; Scarano and Sobrino, 2015).

$$SVF = \frac{1}{\pi}\int_{0}^{2\pi}[\cos\beta\cos^{2}\varphi + \sin\beta\cos(\phi-\alpha)(90-\varphi-\sin\varphi\cos\varphi)]d\phi$$

Equation (4)

Where β and α are surface slope angle and surface aspect calculated from DEM, respectively; φ is the horizon angle; and ϕ is the azimuth direction. The maximum search radius value was set at 200 m, which is the same as Chen (2012).

3.3.2.3. Sky view factor (SVF) photographic analysis

The SVF was also analyzed by photographic methods for verification of the simulation results. Measurements were made at 25 points (16 points in apartment areas and 9 points in multi-family housing areas) in between buildings. The analytical equipment included a Sigma 8 mm f3.5 Circular fisheye lens with 180° angle of view and a Nikon D810 full frame DSLR for full circle image. A compass for the orientation of the photos (Sunnto compass) and a bubble level for the camera (Horusbennu bubble) were also used in analysis. Measurements of air temperature (Test175 H1 with wrapping foil for blocking radiation) and wind speed (Kestrel 4500) were also conducted (Table 6 and Figure 11).

The results of the fisheye photo were arrived at by dividing into sky and structure in a photoshop program and extracting the black and white images. The final photographic SVF value

was calculated by the SOLWEIG model (Lindberg et al., 2008) using the processed fisheye photo.

Many programs are used in SVF calculation, such as Rayman, BM sky, Sky Helios, ArcView SVF-Extension, and Steyn. SOLWEIG is one of the models for calculating the SVF on the basis of a shadow casting algorithm as introduced by Ratti and Richens (1999). It has been widely used in many previous studies (Lindberg, 2010; Konarska, 2014; White and Langenheim, 2014). One characteristic is that the SOLWEIG model value is slightly higher than other models (Hammerle, 2011). The setting of the resolution is 1x1 m as in previous studies. The results of processing are used in the verification by linear regression between the simulated value and photographic value.

Figure 11. Equipments for measurement

Table 6. Technical specs of equipments

Equipment	Spec
Sigma 8mm f3.5 Circular fisheye lens	-Lens Construction:11 Elements in 6 Groups -Angle of View: 180° -Mininum Aperture: f22 -Minimum Focusing Distance: 13.5 cm
Nikon D810 fullframe DSLR	-Effective Pixels (Megapixels): 36.3 million -Sensor Size: 35.9mm x 24mm
Sunnto Tandem compass	-Accuracy: 1/3° -Graduation interval: 0.5° -Scale: Azimuth 360°, Reversed 360°
Horusbennu buble level HCL-1	-Size: 2.4 x 2.4 x 2(cm)
Testo 175 H1	1. Temperature -Measuring range: -20 to +55 °C -Accuracy:±0.4 °C (-20 to +55 °C) -Resolution: 0.1 °C 2. Humidity -Measuring range: 0 to 100%rH* -Accuracy: ±2 %RH (2 to 98 %RH) at +25 °C -Resolution: 0.1 %rH
Kestrel 4500	-Operational Range: 0 to 60m/s -Resolution: 0.1 -Accuracy: Larger of 3% of reading or least significant digit

3.3.2.4 Roof (building) coverage ratio and building height analysis

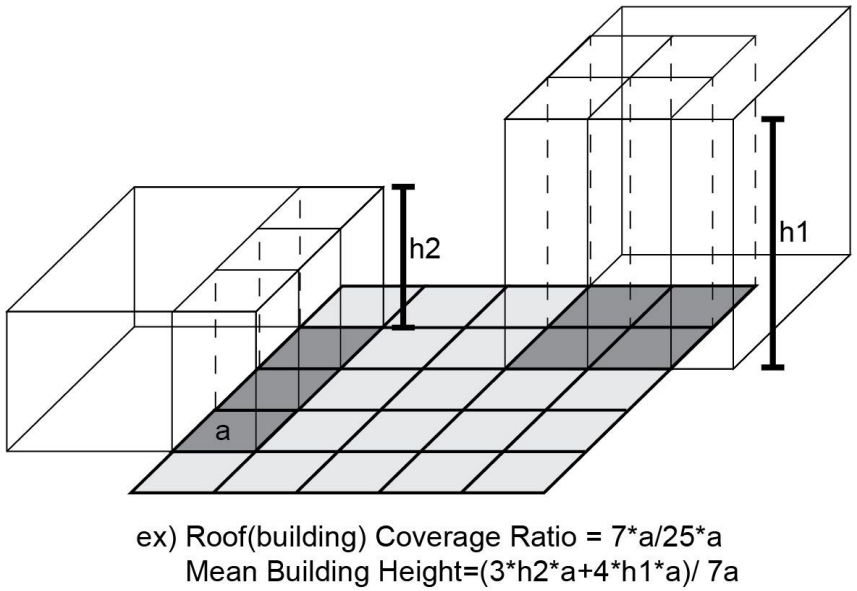

Figure 12. Concept of calculation in roof coverage ratio and building height

In this study, the building form is set as building height and building (roof) coverage ratio. The building coverage ratio is the same as the roof coverage ratio. The building coverage ratio is calculated because the LST has 30 m resolution. The LST values are affected by roof coverage. Therefore, roof coverage has to be included when calculating the LST in an urban canyon. Therefore, in this study, the relationships between the SVF, LST, and building heights by similar roof (building) coverage ratio groups are analyzed. The roof (building) coverage ratio unit is calculated using the 30 m

grid, which is the same as the LST using ArcGIS software. In addition, 2 m raster building data area ratios are calculated in a 30 m grid using zonal statistics.

Building heights are calculated in a similar way; however, each building has a different height. This is divided into a 2 m grid and the average height is calculated for a 30 m grid using zonal statistics (Figure 12).

Residential buildings in Seoul are classified as detached houses, multi-family housing, flat-type apartments, and tower type apartments. These have different building heights. Typically, the highest is a tower type apartment and the lowest is a detached house or multi-family housing. Therefore, the building height is a means of classifying building type.

3.3.3. Statistical analysis

3.3.3.1 Extracting points of building height, SVF, LST

Each pixel from the SVF raster data at the final site is converted to point data. The building height, roof (building) coverage ratio, and LST variables are added on the final site points using ArcGIS. All of the points are extracted at the 95 % level for the total range for the removal of outliers. Areas under 60 % building coverage ratio according to the 30 m

grid for these points were extracted because the maximum building to land ratio in Korea building law is 60 % (Table 7).

Table 7. Regulations of building in residential area by building law ('Ministry of Land, Infrastructure and Transport', 2016)

Division	Maximum number of floors	Floor Area Ratio	Building to Land Ratio
1st Class Exclusive Residential Area	None (Detached house)	Under 100%	Under 50%
2nd Class Exclusive Residential Area	None (Multi-family housing)	Under 150%	Under 50%
1st Class General Residential Area	Under 4 Story (Low rise housing)	Under 200%	Under 60%
2nd Class General Residential Area	Under 7 Story(Detached house), 12 Story(Apartment)	Under 250%	Under 60%
3rd Class General Residential Area	None (High rise housing)	Under 300%	Under 50%

3.3.3.2 Correlation and regression analysis among building height, SVF, LST

The statistical analysis used SPSS, R, and Teraplot software for the correlation analysis and regression analysis for building height, simulated SVF, and LST by roof (building) coverage ratio group. The points are extracted separately by roof (building) coverage ratio and divided into three groups: 0-20%, 20-40%, and 40-60%. Since there are too many points in the 2 m distance resolution, it is difficult to find a specific trend.

Therefore, the SVF axis is split into regular intervals of 0.003, and the mean value of the LST is calculated for each interval. This method is frequently used for the analysis of remote sensing and SVF data in previous studies. A similar approach was followed by Li et al. (2011), Chen et al. (2006), Yuan and Bauer (2007), and Gillies and Carlson (1995). In this way the correlation trend is well expressed. However, point leaning and gathering could not be conducted. Since understanding the correlation was more important than leaning for this study, this method was selected. Regression analysis and correlation analysis between the building height and SVF and the SVF and LST for each similar roof (building) coverage ratio group were conducted. Teraplot software was used to find the relationships between the building height, SVF, and LST by each similar roof (building) coverage ratio group visually.

4. Results and Discussion

4.1. Site selection results

The final site excludes the direct cooling effect range from mountains, green spaces, rivers, and streams. The distribution of the final site is evenly spread throughout Seoul. Excluded areas include apartments nearby the Hangang River, a residential area nearby Junrang-chun (stream), and Anyang-chun (stream). Apartment districts near the big mountain areas, such as Bukhansan Mt., Suraksan Mt., and Achasan Mt. in the north side of Seoul, and Gwanaksan Mt., Cheonggyesan Mt., and Guryongsan Mt. in the south side of Seoul, are excluded too. In addition, areas near green spaces, such as the Seoul forest, the World Cup Park, and Seoul National Cemetery, are excluded.

Even though a conservative standard was used, considerable areas are excluded by the direct effect range of the thermal reduction components. With the distinct characteristics of the topography in Seoul, it is found that considerable areas are influenced by the cooling components. Areas near the Hangang River and Bukhansan Mt. cover a large direct cooling range in residential areas (Figure 13).

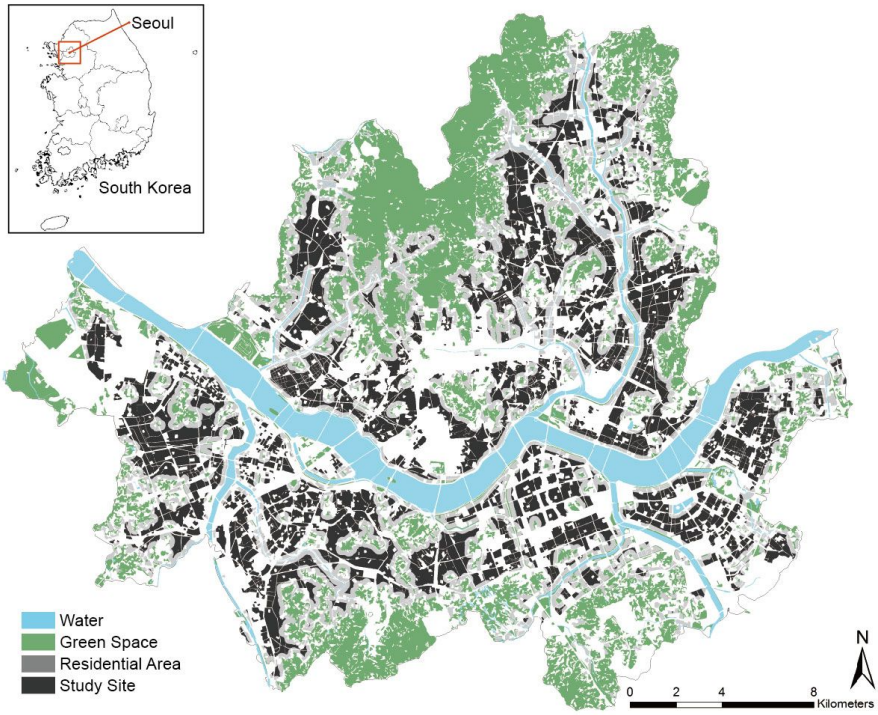

Figure 13. Study site selection results

4.2. Building materials results

4.2.1. Land surface temperature (LST) analysis results

The range of LST is 22.89 ℃-33.91 ℃ with a maximum range of 11 ℃ in the LST in the final site (which excludes the direct range of the cooling components and limited building outdoor space in a residential area) (Figure 14). The value of 11 ℃ value is actually quite large. It considered that land use type was the same and the area was decreased by excluding the direct range of cooling components and only

outdoor space in the residential area. Therefore, other factors, such as building arrangement, density, form, and materials can be found to contribute to different LSTs in equal residential land use areas.

Sukbuk-gu, Yongsan-gu, Yeondungpo-gu, and Guangjin-gu have high values of LST. These areas are far from the Hangang River and the mountains and the ratio of low rise buildings, such as detached houses and multi-family housing, is higher than in other areas (Figure 15). It can be understood that many areas have different LST patterns even though they are in the same borough (Gu). Therefore, the method of monitoring the thermal patterns needs to be specific and include a micro scale approach.

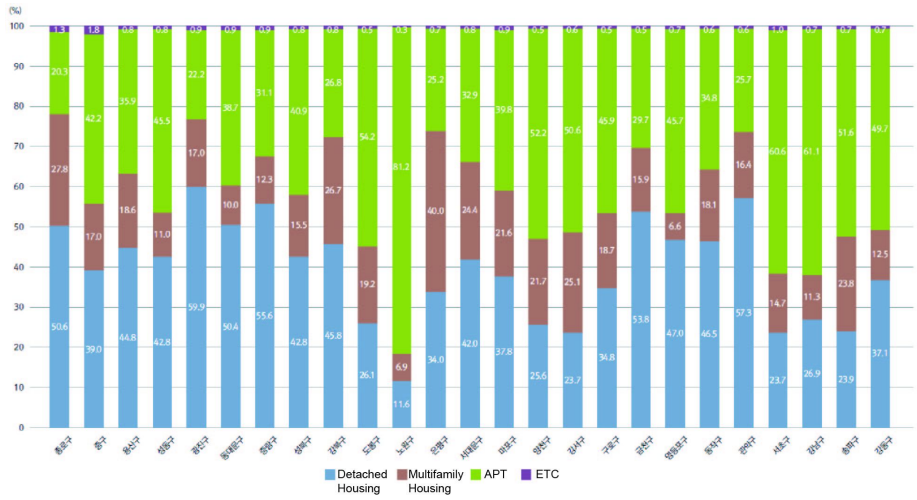

Figure 14. Housing type distribution of Seoul
(Seoul Metropolitan Government, 2015)

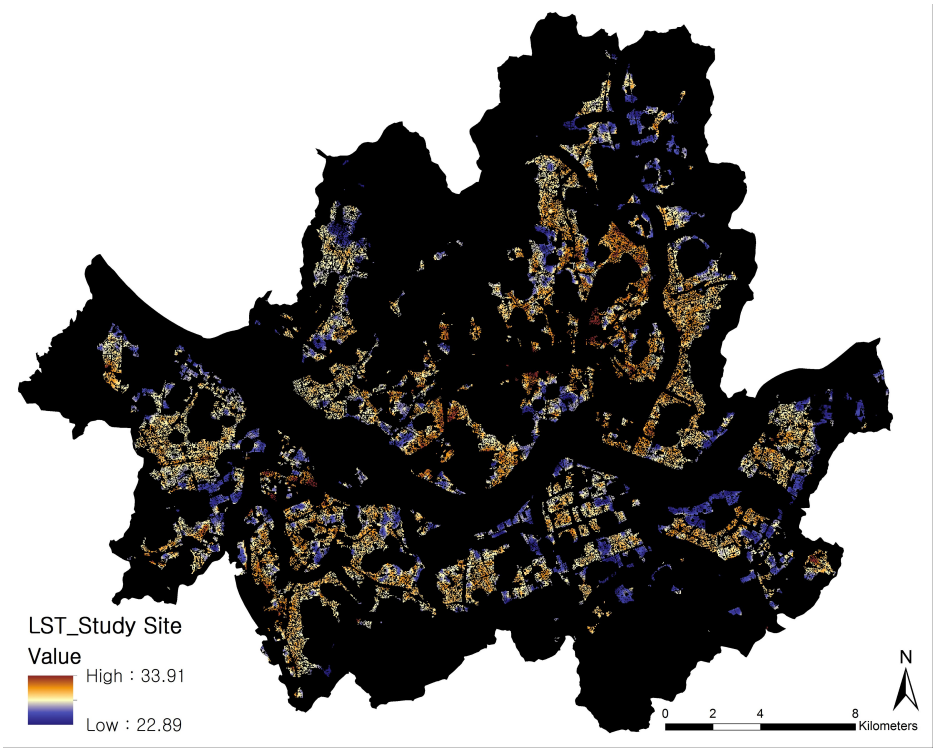

Figure 15. LST distribution in study site

4.2.2. Sky view factor (SVF) simulation analysis results

The results of the SVF calculated by raster-based software methods using high resolution topography (5 m) and a building database (2 m) for all of Seoul are given in Figure 16. These results showed that the SVF is classified according to housing type; low rise detached house, multi-family housing, high rise flat-type apartments, and high rise tower-type apartments. The final site for SVF was extracted from the entire Seoul area.

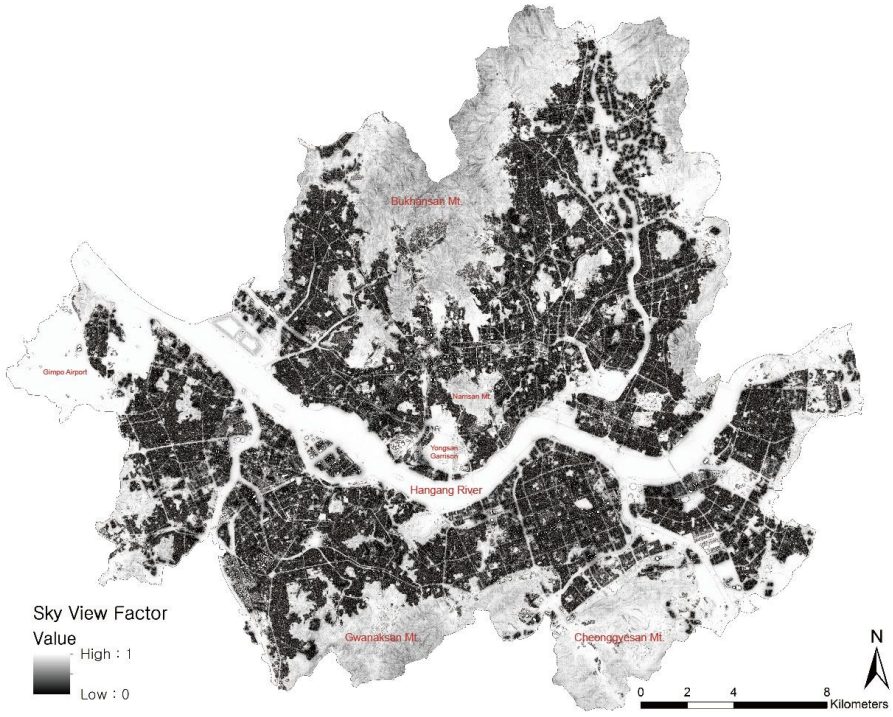

Figure 16. Results of SVF in Seoul by simulation methods

High rise apartments give a relatively low SVF in outdoor spaces, and low rise residential housing, such as detached houses and multi-family housing, lead to relatively high SVFs in outdoor spaces. High rise apartments have different patterns of SVF according to the type of apartment; tower type or flat-type. Tower type apartments are usually taller than flat-type, leading to bigger SVFs because tower type apartments have bigger gaps between each building and smaller shadows than flat-type apartments. They have a thinner and taller form.

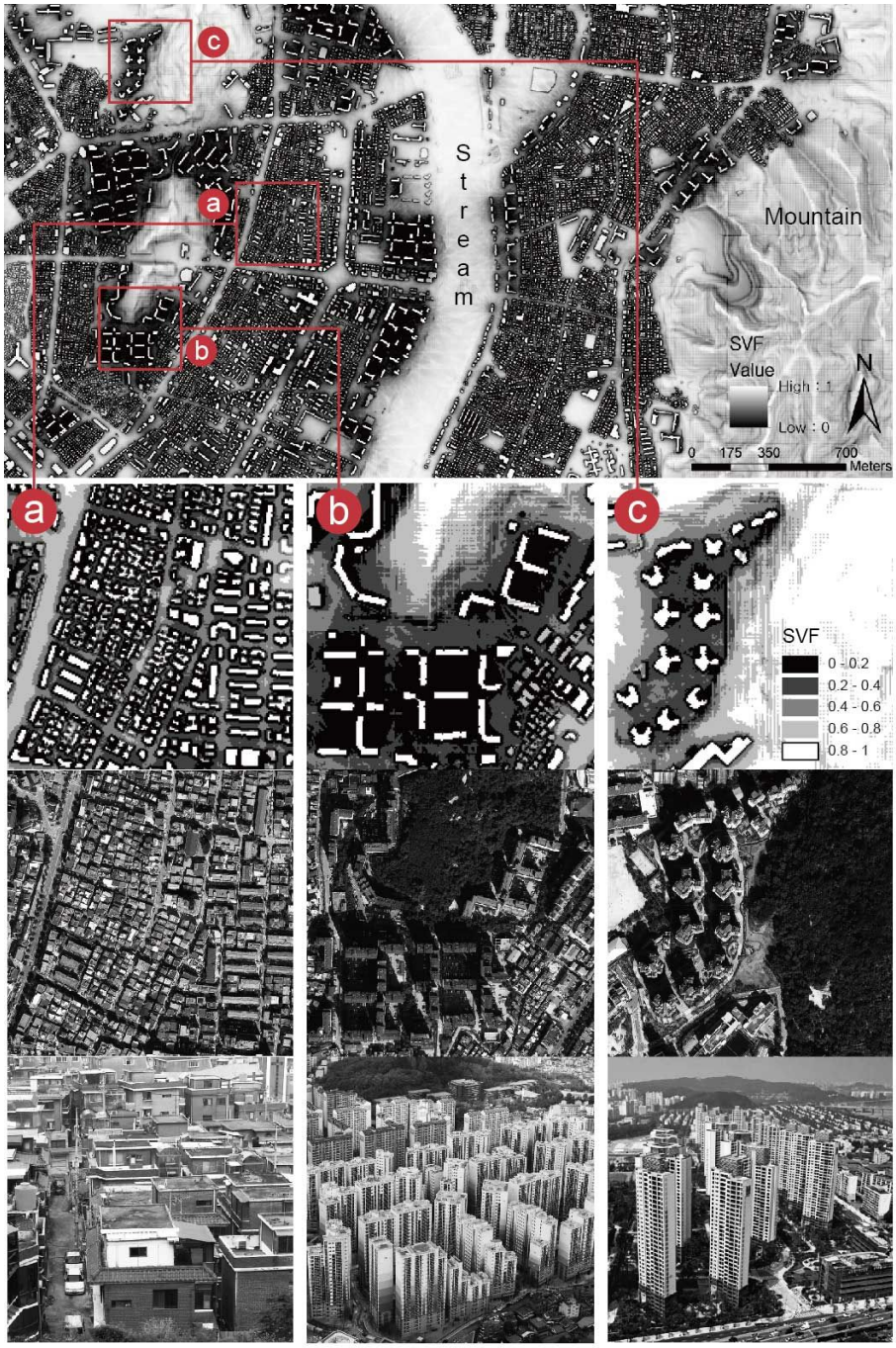

Figure 17. Typical SVF characteristics each housing types
(a: Detached house, multi-family housing, b: Flat-type APT, C: Tower type APT)

The building configuration also leads to different patterns of the SVF even among the same height flat-type apartments. Configurations that are enclosed, such as 'C' forms and 'O' forms, have lower SVFs than do open arrangements, such as 'L' forms and 'I' forms. The SVF in residential areas is also influenced by nearby topography and building heights from commercial buildings (Figure 17).

4.2.3. Sky view factor (SVF) photographic analysis results

Figure 18 shows the processing of selected sky/structures and some of the results. The minimum value of apartments residential areas is 0.15 (15 %) for an 'O' shaped building arrangement. The maximum value is 0.46 (46 %) for the 'L' shaped building arrangement. The range of SVF in multi-family housing areas is from 0.26 (26 %) to 0.52 (52 %). This indicates that building arrangement and height are key factors in apartments in residential areas, and the extent of alleys is a key factor in multi-family residential areas.

The average SVF from the photographic methods is 0.32 in apartment areas and 0.37 in multi-family housing areas. Even if samples are too few for statistical calculations, it can be seen that areas with low building heights have higher SVFs than areas with high buildings. The results of a single regression analysis showed a high R square value (0.977)

between the simulation and photographic methods. Figure 19 shows clearly that the simulation approach is appropriate for SVF analysis.

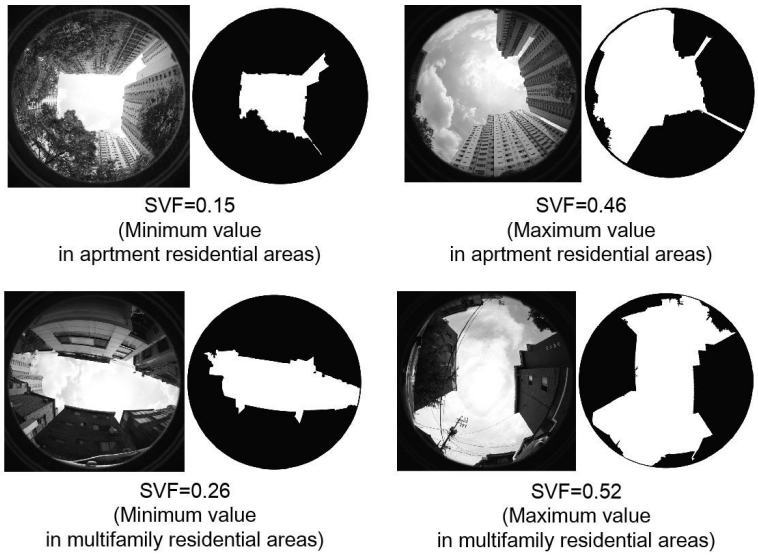

Figure 18. Results of SVF photographic methods

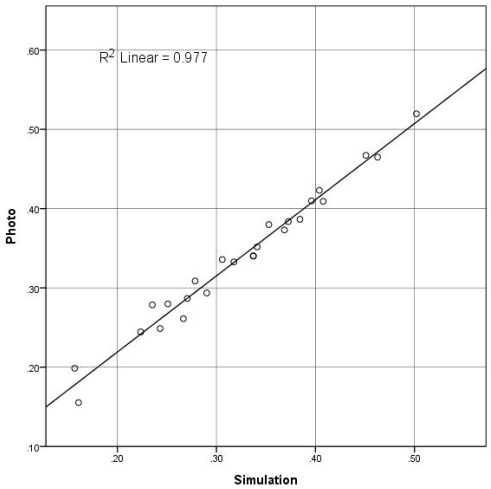

Figure 19. Single linear regression analysis results between simulation and photographic methods

4.2.4. Roof (building) coverage ratio and building height analysis results

The calculated roof (building) coverage ratio and building heights by a 30 m grid are given in Table 8. The section of roof (building) coverage ratio under 60 % is 95.52 % for all points. The points are compared by each roof coverage group (0-20 %, 20-40 %, and 40-60 %). There are more areas with high roof (building) coverage ratios. The overall pattern indicates that the low roof (building) coverage ratio group has a low building height, higher SVF, and lower LST; but the higher roof (building) coverage ratio group has the opposite pattern.

Table 8. Results of SVF, LST, building height distribution by roof coverage ratio group

Roof (building) coverage ratio	0-20%	20-40%	40-60%
Sample percentage (%) (Number of points)	21.79 (3,372,845)	36.54 (5,655,979)	41.67 (6,450,045)
Mean SVF	0.3853	0.3085	0.2238
Mean LST (°C) (min, max)	27.3476 (22.76 / 32.24)	27.98 (22.88 / 33.51)	28.42 (22.89 / 33.91)
Mean building height (m) (min, max)	92.40 (0 / 176.62)	48.97 (0.32 / 180.24)	27.29 (1.96 / 167.68)

4.3. Statistical analysis results

4.3.1. Correlation analysis results between SVF, building height

Points at the 95 % level from the total range were extracted first. Consequently, 99.63 % of the points were selected. Next, points under 60 % in roof (building) coverage ratio based on the Korea residential building law were extracted. This resulted in 95.52 % of the points being selected (15,478,869 points). The correlation analysis between SVF and building height used these points. As a result, these two factors showed a strong quadratic relationship. The overall pattern is a negative correlation, indicating that an increase in building height would lead to a decrease of SVF (Figure 20). These results are similar to Chen (2012) for an analysis in dense urban Hong Kong (Figure 4). These results confirm that low rise buildings, such as detached houses and multi-family housing, lead to high SVF values, and high rise buildings, such as flat-type apartments or tower type apartments lead to low SVF values.

The most unique pattern is an inflection point at around 0.2 in the SVF value. For example, the study of Chen (2012) in Hong Kong showed a linear pattern between building height and SVF; but in this study, there was a quadratic relationship between building height and SVF.

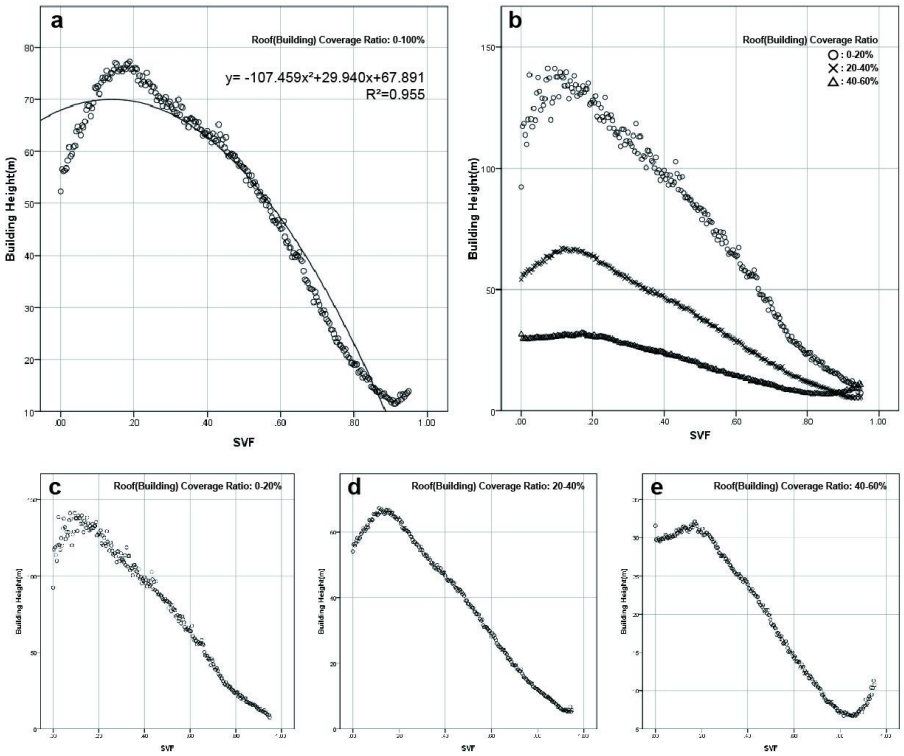

Figure 20. Correlation between building heights and SVF by roof(building) coverage ratio group using mean analysis; SVF axis is split into regular intervals of 0.03 units, for each of which the mean value of LST is calculated
(a: Total, b: By each group, c: 0-20%, d: 20-40%, e: 40-60%)

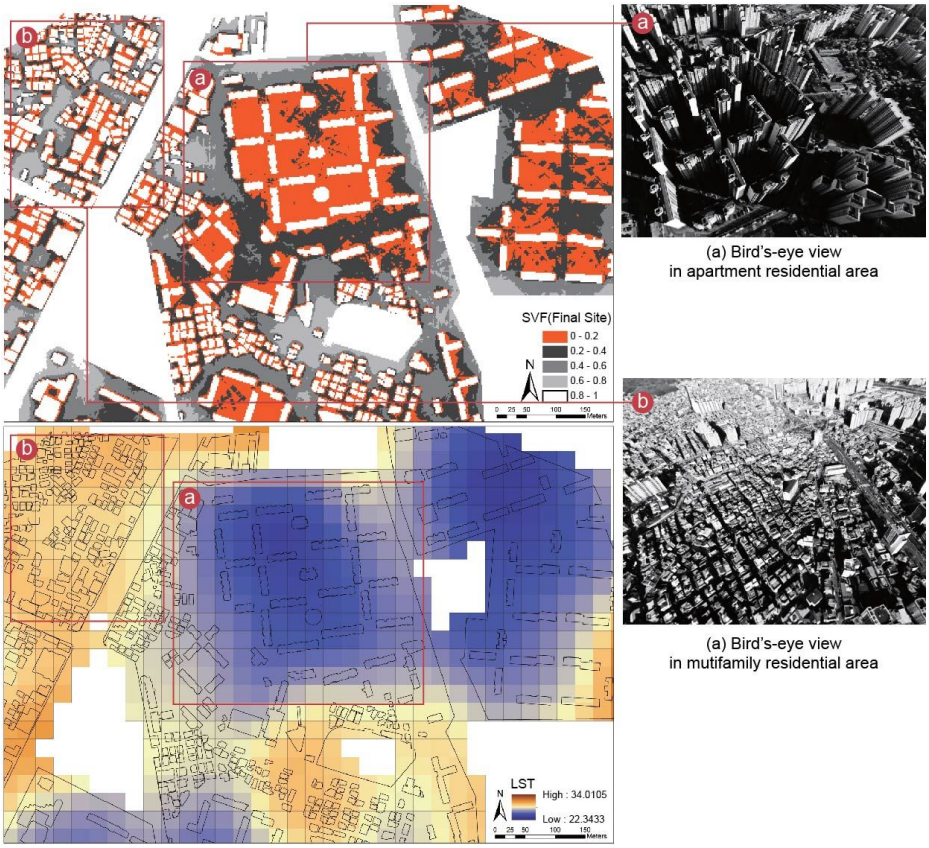

Figure 21. Enlarge under 0.2 SVF area and LST (Red: SVF 0-0.2)

This means that there are sections with different SVF values even if building heights are similar. This section is mostly composed of high rise residential building areas with flat-type or tower type apartments.

The extracted points from the under 0.2 SVF area are shown in Figure 21 to understand the characteristics in this section. The enclosed arrangement of flat-type apartments leads to the 0.2 SVF area through this analysis, and flat-type

apartments result in an overall low LST pattern. The enclosed forms, such as the 'C' or 'O' shapes, lead to lower SVF values than do the open forms, such as the 'L' or 'I' shapes, in the same housing complex. Therefore, this means that in spite of similar building height, building configurations lead to different SVF values in high rise building areas.

This phenomenon more frequently occurs for the over 20 % roof (building) coverage ratio than for the under 20 % group. High building density areas have a greater variation in SVF value than lower building density areas with varying combinations of building configurations. Note that high rise building complexes usually have a high density placement of over 20 %. This trend results in a greater variation in SVF values considering the variation in building configurations in high rise building areas.

4.3.2. Correlation and regression analysis results between SVF, LST

Figure 22 gives the results of the correlation analysis between SVF and the daytime LST for the final site with all points at 2 m of distance. However, as indicated previously, there are too many points (15,478,869 points) generate cloud pattern caused by the 2 m distance. It makes hard to find specific trend.

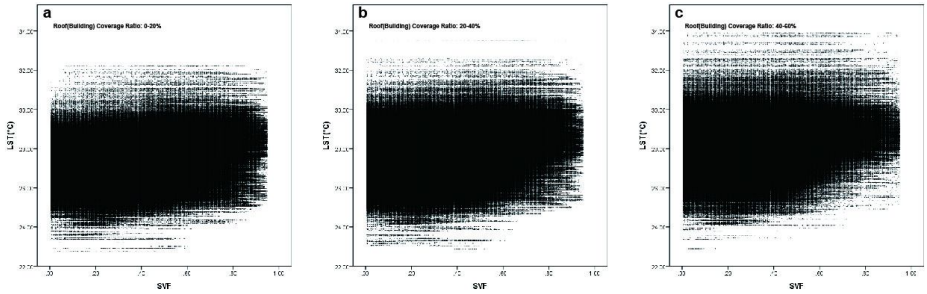

Figure 22. Scatter plot of correlation analysis between LST and SVF by roof(building) coverage ratio group (a: 0-20%, b: 20-40%, c: 40-60%)

After the SVF axis was split into regular intervals, the mean value of LST was calculated. The resulting graph is shown in Figure 23. The X and Y axes are the SVF and mean LST. In this way, the correlation trend is well expressed.

These two factors have a strong quadratic correlation. The overall pattern is a positive correlation, indicating that an increase in SVF would lead to an increase in LST. It is also compare with visually at Figure 21. The graphs are similar for every group of roof (building) coverage ratio. There are maximum ranges of the mean LST for each roof (building) coverage ratio group; 0-20 % (1.61 °C), 20-40 % (1.22 °C), and 40-60 % section (0.69 °C) (Table 8 and Figure 23).

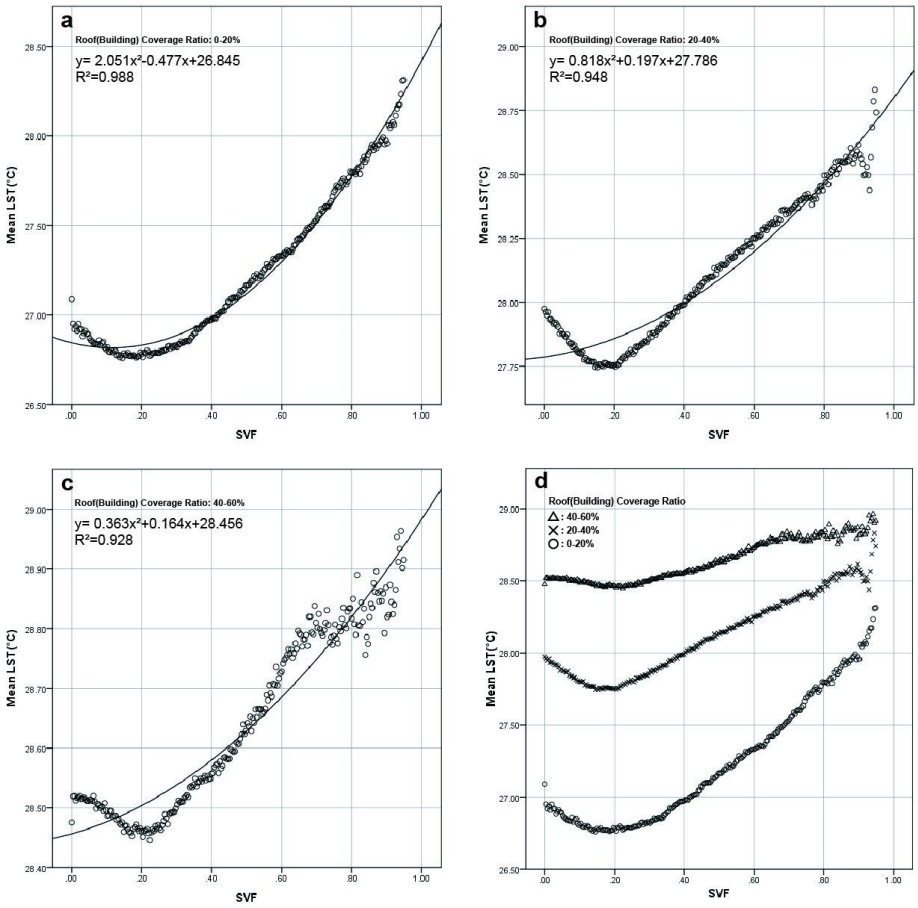

Figure 23. Correlation between LST and SVF by roof(building) coverage ratio group using mean analysis (a: 0-20%, b: 20-40%, c: 40-60%, d: By each group)

The quantitative range of the mean LST is small caused by the mean value from a large range of LST, restricting land use type to only residential areas. There was an obvious positive correlation between SVF and LST considering this limitation. These results are similar to those from Scarano and Sobrino (2015) (Figure 6) that deal with simulated SVF and

LST. However, they did not consider the land use and roof (building) coverage ratio. The graph showed significantly that increasing SVF leads to increasing LST in the low roof (building) coverage ratio group compared to the other groups.

Low rise buildings, such as detached houses and multi-family housing, lead to high SVF; and this high SVF leads to high LST in outdoor spaces. Therefore, low rise residential building areas are the most vulnerable in a daytime thermal environment. High rise residential building areas, such as flat-type or tower type apartments, have lower LSTs than the low rise building areas.

The most unique pattern is an inflection point at around 0.2 in SVF value, similar to the results with building height. This is similar to the results of Giridharan (2006) using photographic methods in Hong Kong. They found tiny inflection points near the 0.2 SVF value on clear summer days. This previous study did not show a clear correlation because of limited samples in Hong Kong (Figure 25).

The overall pattern is a positive correlation showing that increasing SVF leads to increasing LST for SVF over 0.2 caused by increasing direct solar radiation in the daytime. In contrast, increasing SVF leads to decreasing LST for SVF values under 0.2. This pattern is seen for every roof (building) coverage ratio group.

Based on further analysis in this study, most of the area

with under 0.2 SVF value is in an enclosed type arrangement, such as a 'C' or 'O' shape from a flat-type apartment. It is known that low value of SVF lead to increasing LST in the nighttime. In this study, extremely low values of SVF increase the LST even in the day time for high rise enclosed type buildings.

This low SVF area expected relatively higher temperatures than the other areas in the nighttime by decreasing radiant cooling and increasing counter radiant, stored heat. Therefore, SVF values under 0.2 that occur in enclosed type arrangements in high rise flat-type apartment should be avoided for their thermal environment.

An increasing SVF led to increasing mean LST for SVF values over 0.2 in every roof (building) coverage ratio group. The increasing rate of mean LST is higher in the low roof (building) coverage ratio group compared to the other roof (building) coverage ratio groups. In other words, the increasing rate of LST by SVF is higher in for low density building areas because the range of quantity change in radiation is smaller in high density building areas with a smaller sized urban canyon. The results of the regression analysis between the SVF and the mean LST for every group of roof (building) coverage ratio show a similar quadratic form with R square values greater than 0.9. Therefore, the trend of LST with SVF is described well by these graphs (Figure 23).

4.3.3. Correlation analysis results among SVF, Building height and LST

The goal of this study was to find correlations among building forms, the urban canyon form created by buildings, and the thermal environment in the urban canyon. To meet this goal, this study focused on correlations with building height, SVF, and LST by each similar roof (building) coverage ratio group at intervals of 20 % using 3-D graphs. The results are given in Figure 24. This graph showed an overall pattern that increasing building height led to decreasing SVF and decreasing LST in every section where SVF values were over 0.2.

However, the building height also rebounded for SVF values under 0.2. This means that buildings with the same height can have different SVF values according to their configuration. In addition, the LST pattern rebounds around the SVF 0.2 value in every group. The range of rebound for the LST is the highest for the 20-40 % roof (building) coverage ratio.

Therefore, through this analysis, increasing building heights lead to decreasing SVF, which leads to decreasing LST through decreasing direct solar radiation, irrespective of building density. The correlation between LST and SVF is positive over SVF 0.2 and negative under SVF 0.2. In addition, the range of changing LST is greater in the 0-40 %

roof (building) coverage ratio group than in the 40-60 % group. The radiation quantity change in high density building areas is smaller than in low density areas because of a smaller urban canyon. This leads to small changes in LST in high density building areas.

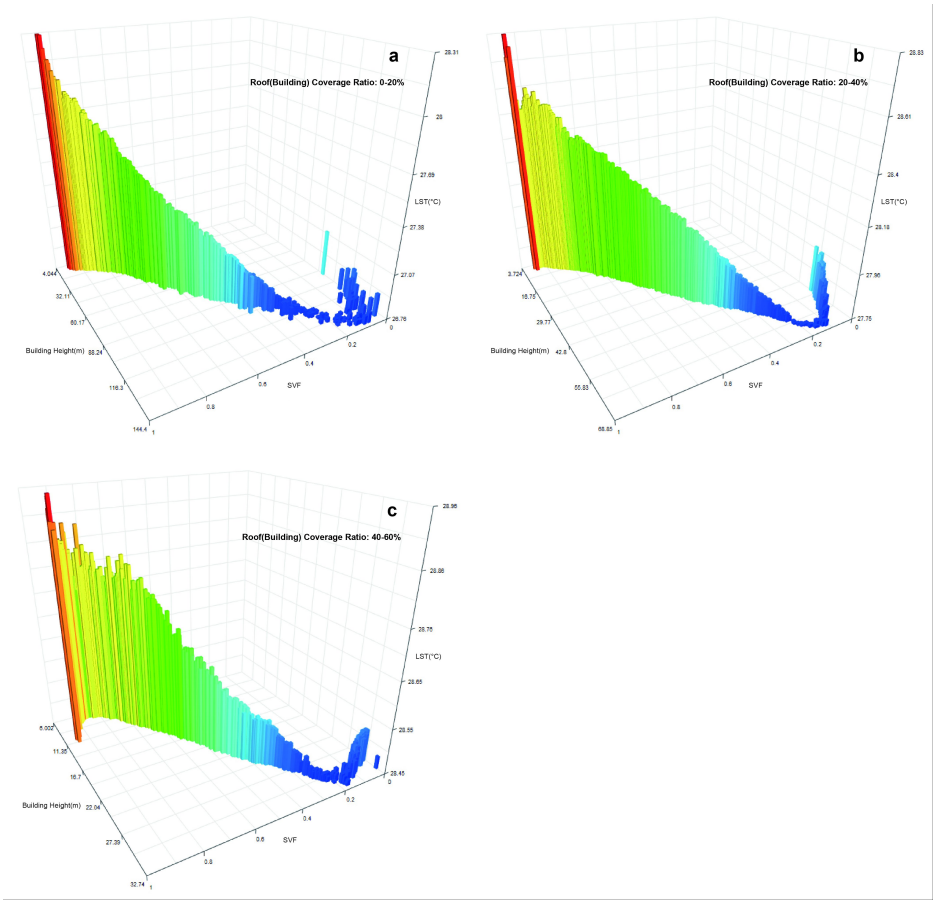

Figure 24. Correlation among LST, SVF, building height by roof (building) coverage ratio group (x axis: SVF, y axis: building height, z axis: LST)

5. Discussion

The overall pattern is a positive correlation between SVF and LST in daytime. This is similar to previous studies. However, in mostly studies, they did not observe a negative correlation in extremely low SVF sections.

The closest results to this study are from Giridharan (2006) regarding a correlation between SVF and UHI in Hong Kong. According to this study, it was found that SVF and UHI had a positive relationship in section with an SVF value over 0.2. In addition, there were negative correlations in areas with an SVF value under 0.2 (Figure 25). These results compare well with the results in this study.

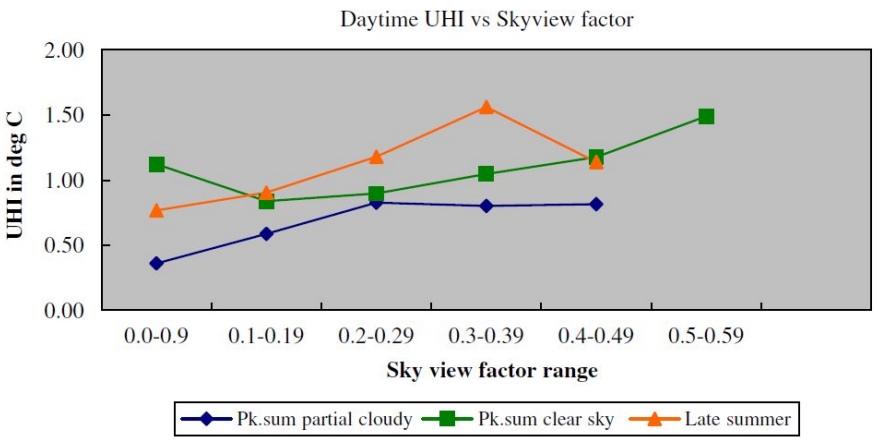

Figure 25. Results of correlation between UHI and SVF in Hongkong (Green: daytime condition in clear sky) (Giridharan et al., 2006)

The results are similar because of the similar environments between high-rise build up in Hong Kong and the high-rise apartment housing areas in Korea. According to the results in this study, an 'O' shape results in low SVF values for by high-rise flat-type apartments. One explanation is that the increasing surface heat balance forms stored heat and counter radiation due to declining long wave radiation caused by obstacles in the nighttime that are still having an effect in the daytime in areas where SVF is under 0.2. The Landsat 8 LST time is 11 a.m., which does not provide enough sun elevation for incoming direct solar radiation to the ground for the small SVF value of this area. These reasons lead to a nighttime thermal pattern still existing in daytime when SVF is under 0.2.

In previous studies, most survey on sample sites. However, there are limitations that can be overcoming by remote sensing. For example, He (2015) developed a correlation between air temperature and SVF in clear daytime in summer in China (Figure 26). He found that the low SVF value section had a relatively high temperature in the nighttime caused by declining long wave radiation. The pattern of this study did not show a dramatic turn around in nighttime patterns as did He (2015). However, there are slightly rising LSTs in section with SVF values lower than 0.2. This is likely because this study dealt with daytime at 11 a.m. This time is during the

process of changing the thermal pattern from nighttime to daytime considering the Landsat measure time.

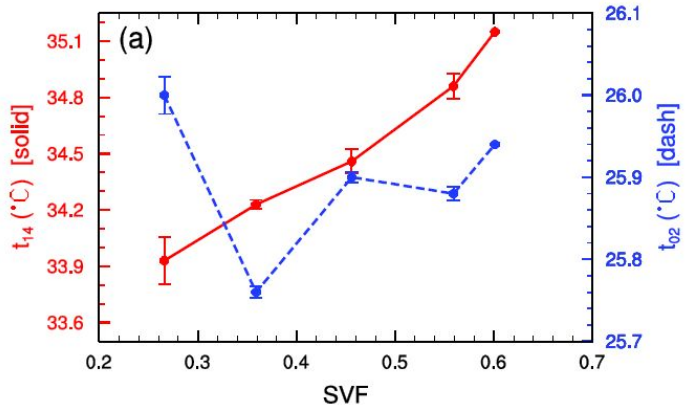

Figure 26. Temperature pattern of day and night in clear summer (Red: Day, Blue: Night) (Xiaodong et al., 2015)

In addition, the under 0.2 SVF area may have lower green space than does the over 0.2 SVF area. In a previous study by Moon (2011), it was found that the courtyards of enclosed arrangement, such as 'C' or 'O' shape arrangements of flat-type apartments, were used more as parking lots having lower green space. This area also trapped heat with the arrangement of the apartments. Therefore, the courtyard air temperature is relatively high even though a lot of shadow area is present. In this study, an analysis of the correlation between NDVI and SVF focused on the under 0.2 SVF area. The NDVI is a numerical indicator that uses the visible and near-infrared bands of the electromagnetic spectrum and is

adopted to analyze remote sensing measurements and assess whether the target being observed contains live green vegetation. Calculations of NDVI for a given pixel always result in a number that ranges from minus one (-1) to plus one (+1); however, no green leaves gives a value close to zero (Holme et al., 1987; USGS, 2015).

$$NDVI = \frac{NIR - RED}{NIR + RED} \qquad \text{Equation (5)}$$

In previous studies, the correlation between NDVI and LST revealed that increasing NDVI leads to decreasing LST (Hang et al., 2009; Li et al., 2012). In this study, the correlation between SVF and NDVI was conducted with the final site points. There was a separate analysis by each 20 % roof (building) coverage ratio group. The range of NDVI in residential areas is around 0-0.4. In general, the NDVI values are accounted for as small vegetation (0.2-0.3), medium vegetation (0.3-0.4), and high vegetation (over 0.4) (Tilahun, 2015). Therefore, the range of results is reasonable regarding the characteristics of residential areas in an urban setting. The results showed that the residential area correlation between NDVI and LST is negative in every roof (building) coverage ratio group (Table 9 and Figure 27 a,b,c). This is the same as in previous studies.

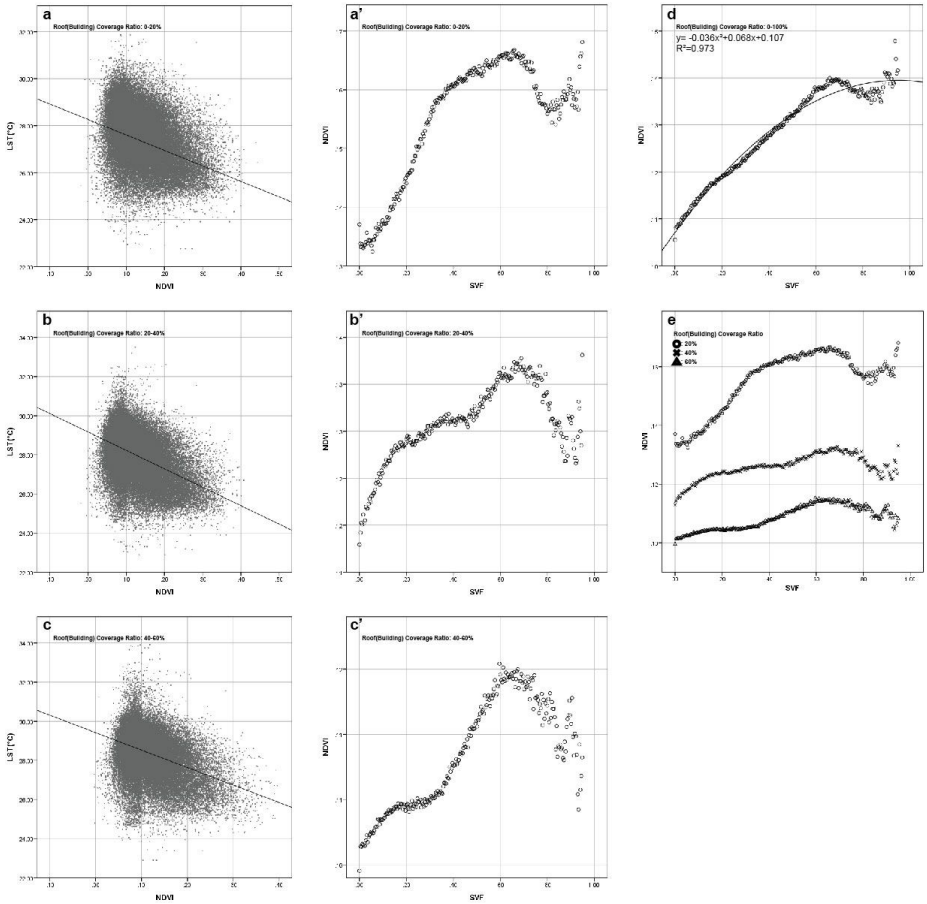

Figure 27. Correlation among LST, NDVI, SVF by roof (building) coverage ratio group
a, b, c: Correlation between LST and NDVI by roof coverage ratio group
a', b', c': Correlation between NDVI and SVF by roof coverage ratio group
(a, a': 0-20%, b, b': 20-40%, c, c': 40-60%)
d / e: Correlation between SVF and NDVI in total / By group

Table 9. Results of NDVI distribution by roof (building) coverage ratio group

Roof (building) coverage ratio	0-20%	20-40%	40-60%
Sample Percentage (%) (Number of points)	21.79 (3,372,845)	36.54 (5,655,979)	41.67 (6,450,045)
Mean NDVI (NDVI min, max)	0.1479 (-0.0187 / 0.4440)	0.1248 (-0.0187 / 0.4076)	0.1086 (-0.0032 / 0.3960)

The results show that NDVI and SVF have a positive relationship for all of the SVF values in every group (Figure 27 a',b',c'). This means that increasing outdoor space leads to increases in green space quantity and quality. With the use of outdoor space in residential area as parking lots and green space, this positive relationship is reasonable.

For the under 0.2 SVF sections, the NDVI increasing ratio is higher than in the other sections. Generally, in the under 0.2 SVF sections, the building form is an enclosed type arrangement, meaning that the use of the enclosed courtyard is more frequently as a parking lot than green space.

To summarize, the under 0.2 SVF section has a pattern that with increasing SVF, the NDVI increases and LST decreases. The LST is influenced by increasing NDVI in this section. However, the increasing SVF leads to increasing NDVI and increasing LST in the over 0.2 SVF section. This is because of the increase in direct solar radiation even though there is an increasing NDVI (Table 9).

6. Conclusion

The ‘Urban Heat Island (UHI)’ can lead to negative effects on human health and quality of life. Therefore, the monitoring of UHI is important for sustainable development in urban planning. Building geometry is one of the key factors for the causes of UHI. High density structures in highly urbanized cities seriously affect the thermal condition. Many previous studies have limitations in their methods for acquiring the values of SVF and thermal condition at city scale. In these studies, the thermal characteristics for land use and the cool island effect are not considered.

Therefore, this study focused on the relationship among building form, urban canyon by building form, and the outdoor thermal environment. Correlations with building heights, simulated SVF, and LST by roof (building) coverage ratio group were made using a SVF simulation technique and remote sensing considering roof (building) coverage ratio.

The simulated SVF and LST are useful methods for city scale measurements. Recently, some studies evaluated the correlation between simulated SVF and LST for understanding the thermal condition, but there are limitations. First, LST has very different temperature patterns by land use, but it is not evaluated in those studies. Second, the roof (building) ratio

needs to be evaluated in measuring the thermal condition in building outdoor space. Those studies did not consider this because the Landsat 8 TIRS band has a 30 m resolution. Third, the distance from a thermal reduction component is an important factor because mountains, rivers, and green spaces have a cooling effect. In addition, the different types of land use have unique thermal characteristics. However, these factors were not considered in previous studies and need to be evaluated. Previous studies also did not understand the effect of building arrangement on the thermal condition.

Therefore, this study analyzed the correlations of building heights, SVF, and LST by roof(building) coverage ratio group using SVF simulation technique and remote sensing. In addition, this study analyzed mechanisms discussed in previous studies and evaluated the distribution of green space in residential areas using NDVI index. The study site was limited to residential areas to evaluate land.

The focus of the study was on residential areas since the thermal comfort of a residential area directly affects vulnerable people, such as children and the elderly. In this analysis, components directly affecting the thermal reduction, such as mountains, the Hangang River, streams, and green space, were considered. To find organic relationships among building height, the SVF in outdoor space, and LST, comparisons were made within similar roof (building) coverage

ratio groups to control the problem caused by the limitation of LST resolution.

To summarize, low-rise buildings, such as detached houses and multi-family housing, result in a high SVF condition. A high SVF results in a high LST caused by increasing net radiation near the ground because of increased direct solar radiation. In contrast, high-rise buildings, such as flat-type or tower type apartments, result in a low SVF in the urban canyon and provides a low LST environment.

Within a large area, there are sections with different SVF values, even for buildings with similar height in high-rise building areas. This was caused by the arrangement of high rise flat-type apartments. A value of 0.2 for SVF is an inflection point. The extracted area with SVF values under 0.2 in the simulated data represents an enclosed type arrangement, such as a 'C' or 'O' shape. Open type arrangements, such as 'L' or 'I' shapes, have SVF values mostly over 0.2. In addition, the SVF and LST have a negative correlation for areas with SVF values under 0.2, such as those with enclosed building arrangements. This negative correlation is expected due to a decline in radiant cooling ability at night caused by the low SVF in spite of the daytime conditions. Therefore, enclosed type high rise buildings should be avoided in urban planning.

This pattern for sections with SVF values under 0.2 is

unique. Based on previous studies, a small SVF value area leads to a decline in long-wave radiation increasing counter radiation in the nighttime. Therefore, not cooling the surface in the nighttime still influences daytime surfaces. The Landsat 8 LST is observed on site at 11 a.m. when the elevation of the sun is not high enough to heat the surface in a low SVF area. Therefore, in under 0.2 SVF areas, there is not enough direct solar radiation on the surface so the nighttime pattern still appears in the daytime.

Conversely, an area with SVF value under 0.2 has lower green space than areas with SVF over 0.2. In previous studies, Moon (2011) found that courtyards in enclosed arrangement flat-type apartment have more parking lots and less green space than the other configurations. Therefore, a correlation analysis between NDVI and SVF focused on areas with SVF values under 0.2. The results showed that NDVI and SVF have a positive relationship over all SVF values. In sections with SVF under 0.2, the increasing NDVI ratio is higher than in the other sections. For SVF values under 0.2, as SVF increased, NDVI increased while LST decreased. The increase in NDVI decreases LST. In contrast, in areas where SVF is over 0.2, as SVF increased, NDVI increased, and LST increased. This pattern means that the mechanism of increasing direct solar radiation affects the increase of NDVI. This study found quantitative correlations among building

forms, the urban canyon, and the thermal environment using simulated SVF based on high resolution data and remote sensing. This study can used basic data from urban planning or building construction. Ultimately, it can contribute to sustainable development.

7. References

Abineh Tilahun. (2015), Application of GIS for Calculate Normalize Difference Vegetation Index (NDVI) using LANDSAT MSS, TM, ETM+ and OLI_TIRS in Kilite Awulalo, Tigray State, Ethiopia, Journal of Environment and Earth Science, Vol.5, No.3

Baker, W.L. and Y. Cai., (1992), The r. le Programs for Multiscale Analysis of landscape Structure Using the GRASS Geographical Information System, Landscape Ecology, 7, 291-302

Baker, L. A., Brazel, A. J., Selover, N., Martin, C., McIntyre, N., Steiner, F. R. and Musacchio, L. (2002). Urbanization and warming of Phoenix (Arizona, USA): Impacts, feedbacks and mitigation. Urban ecosystems, 6(3), 183-203.

Barring, L., Mattsson, J. O., and Lindqvist, S. (1985). Canyon geometry, street temperatures and urban heat island in Malmö, Sweden. Journal of Climatology, 5(4), 433-444.

Bechtel, B., Alexander, P. J., Böhner, J., Ching, J., Conrad, O., Feddema, J., ... and Stewart, I. (2015). Mapping local climate zones for a worldwide database of the form and function of cities. ISPRS International Journal of Geo-Information, 4(1), 199-219.

Böhner, J., and Antonić, O. (2009). Land-surface parameters specific to topo-climatology. Developments in soil science, 33, 195-226.

Holmer, B., Thorsson, S., and Eliasson, I. (2007). Cooling rates, sky view factors and the development of intra-urban air temperature differences. Geografiska Annaler: Series A, Physical Geography, 89(4), 237-248.

Brohan, P., Kennedy, J. J., Harris, I., Tett, S. F., and Jones, P. D. (2006). Uncertainty estimates in regional and global observed temperature changes: A new data set from 1850. Journal of Geophysical Research: Atmospheres, 111(D12).

Blacker, S. (2009). From Outer Space to Green Space: An object oriented approach to classifying urban green space in Kuala Lumpur.

Blaschke, T. (2010). Object based image analysis for remote sensing. ISPRS journal of photogrammetry and remote sensing, 65(1), 2-16.

Buyadi, S. N. A., Mohd, W. M. N. W., and Misni, A. (2013). Green spaces growth impact on the urban microclimate. Procedia-Social and Behavioral Sciences, 105, 547-557.

Buyantuyev, A., and Wu, J. (2010). Urban heat islands and landscape heterogeneity: linking spatiotemporal variations in surface temperatures to land-cover and socioeconomic patterns. Landscape Ecology, 25(1), 17-33.

Byrne, J., Sipe, N., and Dodson, J. (2014). Australian environmental planning: Challenges and future prospects. Routledge.

Chapman, L., Thornes, J. E. and Bradley, A. V. (2001). Rapid determination of canyon geometry parameters for use in surface radiation budgets. Theoretical Appl. Climatol., 69: 81-89.

Chapman, L., Thornes, J. E., and Bradley, A. V. (2002). Sky-view factor approximation using GPS receivers. International Journal of Climatology, 22(5), 615-621.

Chapman, L., and Thornes, J. E. (2004). Real-time sky-view factor calculation and approximation. Journal of Atmospheric and Oceanic Technology, 21(5), 730-741.

Chen, X. L., Zhao, H. M., Li, P. X., and Yin, Z. Y. (2006). Remote

sensing image-based analysis of the relationship between urban heat island and land use/cover changes. Remote sensing of environment, 104(2), 133-146.

Chen, L., Ng, E., An, X., Ren, C., Lee, M., Wang, U., and He, Z. (2012). Sky view factor analysis of street canyons and its implications for daytime intra-urban air temperature differentials in high-rise, high-density urban areas of Hong Kong: a GIS-based simulation approach. International Journal of Climatology, 32(1), 121-136.

Connors, J. P., Galletti, C. S., and Chow, W. T. (2013). Landscape configuration and urban heat island effects: assessing the relationship between landscape characteristics and land surface temperature in Phoenix, Arizona. Landscape ecology, 28(2), 271-283.

Deroisy, B. (2013). Daylight and solar access at urban scale: a methodology and its application to a high density develoment in brussels.

Eliasson, I. (1990). Urban geometry, surface temperature and air temperature. Energy and buildings, 15(1-2), 141-145.

Eliasson, I. (1992). Infrared thermography and urban temperature patterns. In- ternational Journal of Remote Sensing, 13(5), 869-879.

Gal, T., Lindberg, F., and Unger, J. (2009). Computing continuous sky view factors using 3D urban raster and vector databases: comparison and application to urban climate. Theoretical and applied climatology, 95(1-2), 111-123.

Gillies, R. R., and Carlson, T. N. (1995). Thermal remote sensing of surface soil water content with partial vegetation cover for incorporation into climate models. Journal of Applied Meteorology, 34(4), 745-756.

Giridharan, R., Lau, S. S. Y., Ganesan, S., and Givoni, B. (2007).

Urban design factors influencing heat island intensity in high-rise high-density environments of Hong Kong. Building and Environment, 42(10), 3669-3684.

Hang, J., Sandberg, M., and Li, Y. (2009). Age of air and air exchange efficiency in idealized city models. Building and Environment, 44(8), 1714-1723.

Hämmerle, M., Gál, T., Unger, J., and Matzarakis, A. (2011). Introducing a script for calculating the sky view factor used for urban climate investigations. Acta Climatol Chorol, 44, 83-92.

He, X., Miao, S., Shen, S., Li, J., Zhang, B., Zhang, Z., and Chen, X. (2015). Influence of sky view factor on outdoor thermal environment and physiological equivalent temperature. International journal of biometeorology, 59(3), 285-297.

Hong, C. H., and Park, J. H. (2009). Accuracy Improvement of Vegetation Classification Using High Resolution Imagery and OOC Technique. Journal of Environmental Impact Assessment, 18(6), 387-392.

Holm, A. M., Burnside, D. G., and Mitchell, A. A. (1987). The development of a system for monitoring trend in range condition in the arid shrublands of Western Australia. The Rangeland Journal, 9(1), 14-20.

Holmer, B., Thorsson, S., and Eliasson, I. (2007). Cooling rates, sky view factors and the development of intra-urban air temperature differences. Geografiska Annaler: Series A, Physical Geography, 89(4), 237-248.

Jee, J. B., Lee, K. T., and Choi, Y. J. (2014). Analysis of land surface temperature from MODIS and Landsat satellites using by AWS temperature in capital area. Korean Journal of Remote Sensing, 30(2), 315-329.

Jung, G. S., Koo, S., and Yoo, H. H. (2011). Temperature change analysis for land use zoning using Landsat satellite imagery. Journal of Korean Society for Geospatial Information System, 19(2), 55-61.

Karlsson, I. M. (2000). Nocturnal air temperature variations between forest and open areas. Journal of applied meteorology, 39(6), 851-862.

Kim, J. H., and Choi, J. H. (2014). Aanalysis the Structure of Heat Environment in Daegu Using Landsat-8. Journal of the Korean Society of Surveying, Geodesy, Photogrammetry and Cartography, 32(4_1), 327-333.

Kim, M. S., (2002), Assessment of urban green space connectivity and potential dispersal of wildlife from landscape ecological perspective, Seoul University graduate school

Kim, G. G., (2003), Detecting spatial autocorrelation and using spatial regression, Korean journal of policy analysis and evaluation, 13(1), 273-294.

Konarska, J., Lindberg, F., Larsson, A., Thorsson, S., and Holmer, B. (2014). Transmissivity of solar radiation through crowns of single urban trees—application for outdoor thermal comfort modelling. Theoretical and applied climatology, 117(3-4), 363-376

Kong, F., Yin, H., James, P., Hutyra, L. R., and He, H. S. (2014). Effects of spatial pattern of greenspace on urban cooling in a large metropolitan area of eastern China. Landscape and Urban Planning, 128, 35-47.

Kusaka, H., and Kimura, F. (2004). Coupling a single-layer urban canopy model with a simple atmospheric model: Impact on urban heat island simulation for an idealized case. 気象集誌. 第 2 輯, 82(1), 67-80.

Landsberg, H. E. (1981). The urban climate (Vol. 28). Academic

press.

Lee, K. J., Kwak, J. I., Kim, H. S., Jung, J. M., (2013), Effect on the Thermal Environment of the Surrounding Area due to the Large Scale Green Areaa In Case of Seonjeongneung, Korean Society of Environment and Ecology

Lee, S. H., and Park, S. U. (2008). A vegetated urban canopy model for meteorological and environmental modelling. Boundary-Layer Meteorology, 126(1), 73-102.

Li, J., Song, C., Cao, L., Zhu, F., Meng, X., and Wu, J. (2011). Impacts of landscape structure on surface urban heat islands: a case study of Shanghai, China. Remote Sensing of Environment, 115(12), 3249-3263.

Li, X., Zhou, W., Ouyang, Z., Xu, W., and Zheng, H. (2012). Spatial pattern of greenspace affects land surface temperature: evidence from the heavily urbanized Beijing metropolitan area, China. Landscape ecology, 27(6), 887-898.

Li, Y. Y., Zhang, H., and Kainz, W. (2012). Monitoring patterns of urban heat islands of the fast-growing Shanghai metropolis, China: Using time-series of Landsat TM/ETM+ data. International Journal of Applied Earth Observation and Geoinformation, 19, 127-138.

Li, Z. L., Tang, B. H., Wu, H., Ren, H., Yan, G., Wan, Z., ... and Sobrino, J. A. (2013). Satellite-derived land surface temperature: Current status and perspectives. Remote Sensing of Environment, 131, 14-37.

Lindberg, F. (2005). Towards the use of local governmental 3-D data within urban climatology studies. Mapping Image Sci, 2, 32-37.

Lindberg, F., and Grimmond, C. S. B. (2010). Continuous sky view factor maps from high resolution urban digital elevation

models. Climate Research, 42(3), 177-183.

Lindqvist, S. (1970). Bebyggelseklimatiska Studier (English Summary: Climatological Studies of Built-up Areas): Meddelanden från Lunds universitets geografiska institution. Avhandlingar, LXI. CWK Gleerup. Lund.

Liu, L., and Zhang, Y. (2011). Urban heat island analysis using the Landsat TM data and ASTER data: A case study in Hong Kong. Remote Sensing, 3(7), 1535-1552.

Mallick, J., Kant, Y., and Bharath, B. D. (2008). Estimation of land surface temperature over Delhi using Landsat-7 ETM+. J Indian Geophys Union, 12(3), 131-140.

Mackey, C. W., Lee, X., and Smith, R. B. (2012). Remotely sensing the cooling effects of city scale efforts to reduce urban heat island. Building and Environment, 49, 348-358.

Mansour, R. F. (2012). A robust method for Arabic car plates recognition and matching using chain code. American Journal of Computational and Applied Mathematics, 2(3), 105-111.

Masson, V. (2000). A physically-based scheme for the urban energy budget in atmospheric models. Boundary-layer meteorology, 94(3), 357-397.

Maimaitiyiming, M., Ghulam, A., Tiyip, T., Pla, F., Latorre-Carmona, P., Halik, Ü., ... and Caetano, M. (2014). Effects of green space spatial pattern on land surface temperature: Implications for sustainable urban planning and climate change adaptation. ISPRS Journal of Photogrammetry and Remote Sensing, 89, 59-66.

McGarigal, K., and Marks, B. J. (1995). Spatial pattern analysis program for quantifying landscape structure. Gen. Tech. Rep. PNW-GTR-351. US Department of Agriculture, Forest Service, Pacific Northwest Research Station.

Moon, S. Y., (2011). Temperature reduction effects by layout of green space in apartment complex, Seoul University graduate school

Oliveira, S., Andrade, H., and Vaz, T. (2011). The cooling effect of green spaces as a contribution to the mitigation of urban heat: A case study in Lisbon. Building and Environment, 46(11), 2186-2194.

Oke, T. R. (1981). Canyon geometry and the nocturnal urban heat island: comparison of scale model and field observations. Journal of climatology, 1(3), 237-254.

Oke, T. R. (2006). Instruments and observing methods: Report No. 81: initial guidance to obtain representative meteorological observations at urban sites. World Meteorological Organization, WMO/TD (1250).

Park, J. K., Na, S. I., and Park, J. H. (2010). Analysis of Thermal Characteristics for Areas of Musim Stream in Cheongju City. CNU Journal of Agricultural Science, 37(1), 81-86.

Park, J. H., Cho, G. H., (2014). Examining mophological variations of green space effects for urban heat island mitigation: using Landsat 8 and MODIS data from Ulsan, Journal of the Korean Association of Geographic Information Studies

Patz, J. A., Campbell-Lendrum, D., Holloway, T., and Foley, J. A. (2005). Impact of regional climate change on human health. Nature, 438(7066), 310-317.

Postgård, U., and Nunez, M. (2000). Continuous measurements of sky-view factors along roads and their relationship to air and road surface temperature (Doctoral dissertation, PhD Thesis, Earth Sciences Centre, University of Gothenberg, Gothenburg, Sweden).

Purkis, S. J., and Klemas, V. V. (2011). Remote sensing and global

environmental change. John Wiley and Sons.

Ratti, C., and Richens, P. (1999). Urban texture analysis with image processing techniques. In Computers in Building (pp. 49-64). Springer US.

Reddy, M. A. (2008). Textbook of remote sensing and geographical information systems (p. 453). Hyderabad: BS publications.

Scarano, M., and Sobrino, J. A. (2015). On the relationship between the sky view factor and the land surface temperature derived by Landsat-8 images in Bari, Italy. International Journal of Remote Sensing, 36(19-20), 4820-4835.

Schwarz, N., Schlink, U., Franck, U., and Großmann, K. (2012). Relationship of land surface and air temperatures and its implications for quantifying urban heat island indicators—an application for the city of Leipzig (Germany). Ecological Indicators, 18, 693-704.

Stewart, I. D., and Oke, T. R. (2012). Local climate zones for urban temperature studies. Bulletin of the American Meteorological Society, 93(12), 1879-1900.

Souza, L. C. L., Rodrigues, D. S., and Mendes, J. F. (2003). Sky view factors estimation using a 3D-GIS extension.

Svensson, M. K. (2004). Sky view factor analysis-implications for urban air temperature differences. Meteorological applications, 11(03), 201-211.

Tilahun, A., and Islam, Z. (2015). Google earth for land use land cover change detection in the case of gish abbay sekela, west gojjam, amhara state, Ethiopia. International journal of advancement in remote sensing, gis and geography, 3(2), 80-87.

Tuttle, E. M., Jensen, R. R., Formica, V. A., and Gonser, R. A. (2006). Using remote sensing image texture to study

habitat use patterns: a case study using the polymorphic white-throated sparrow (Zonotrichia albicollis). Global Ecology and Biogeography, 15(4), 349-357

Unger, J. (2008). Connection between urban heat island and sky view factor approximated by a software tool on a 3D urban database. International Journal of Environment and Pollution, 36(1-3), 59-80.

Upmanis, H., and Chen, D. (1999). Influence of geographical factors and meteorological variables on nocturnal urban-park temperature differences--a case study of summer 1995 in Göteborg, Sweden. Climate Research, 13(2), 125-139.

Oke, T., and Voogt, J. (1997). Complete urban surface temperatures. Journal of Applied Meteorology, 9(36), 1117-1132.

Voogt, J. (2007, July). How researchers measure urban heat islands. In United States Environmental Protection Agency (EPA), State and Local Climate and Energy Program, Heat Island Effect, Urban Heat Island Webcasts and Conference Calls.

Watson, I. D., and Johnson, G. T. (1987). Graphical estimation of sky view-factors in urban environments. Journal of Climatology, 7(2), 193-197.

Whiteside, T., and Ahmad, W. (2005, September). A comparison of object-oriented and pixel-based classification methods for mapping land cover in northern Australia. In Proceedings of SSC2005 Spatial intelligence, innovation and praxis: The national biennial Conference of the Spatial Sciences Institute (pp. 1225-1231).

White, M., and Langenheim, L. (2014). Measuring urban canyons with real-time light based sky view factor modelling. Oliveira V, PT Pinho P Batista L, C, M.(Eds.), OurcommonFuture Urban Morphology. FEUP, Porto,

Portugal, 239-304.

Yang, X., and Li, Y. (2015). The impact of building density and building height heterogeneity on average urban albedo and street surface temperature. Building and Environment, 90, 146-156.

Yamashita, S., Sekine, K., Shoda, M., Yamashita, K., and Hara, Y. (1986). On relationships between heat island and sky view factor in the cities of Tama River basin, Japan. Atmospheric Environment (1967), 20(4), 681-686.

Yuan, F., and Bauer, M. E. (2007). Comparison of impervious surface area and normalized difference vegetation index as indicators of surface urban heat island effects in Landsat imagery. Remote Sensing of environment, 106(3), 375-386.

Song, B. G., Park, K. H., and Jung, S. G. (2014). Validation of ENVI-met model with in situ measurements considering spatial characteristics of land use types. Journal of the Korean Association of Geographic Information Studies, 17(2), 156-172.

Yoon, M. H., and Ahn, T. M. (2009). An application of satellite image analysis to visualize the effects of urban green areas on temperature. Journal of the korean institute of landscape architecture, 37(3), 46-53.

Zhang, X., Zhong, T., Feng, X., and Wang, K. (2009). Estimation of the relationship between vegetation patches and urban land surface temperature with remote sensing. International Journal of Remote Sensing, 30(8), 2105-2118.

Zheng, B., Myint, S. W., and Fan, C. (2014). Spatial configuration of anthropogenic land cover impacts on urban warming. Landscape and Urban Planning, 130, 104-111.

Zhou, D., Zhao, S., Liu, S., Zhang, L., and Zhu, C. (2014). Surface urban heat island in China's 32 major cities: Spatial patterns and drivers. Remote Sensing of Environment, 152, 51-61.

8. Appendix (Photographic methods results)

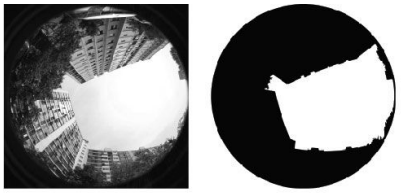

SVF=0.29

SVF=0.38

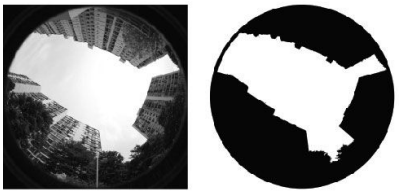

SVF=0.37

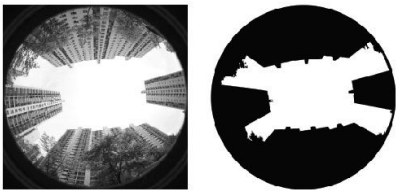

SVF=0.33

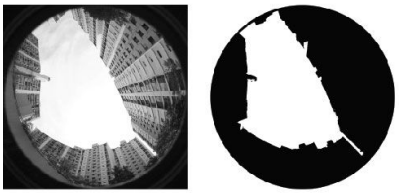

SVF=0.34

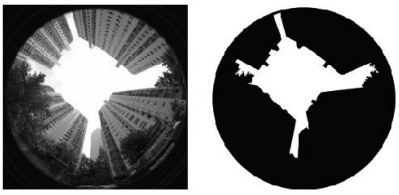

SVF=0.19

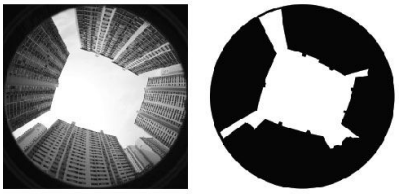

SVF=0.27

SVF=0.30

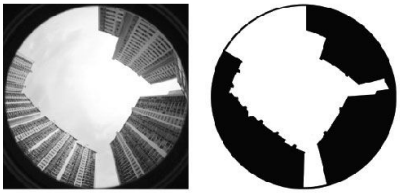

SVF=0.46

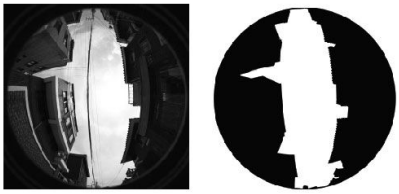

SVF=0.34

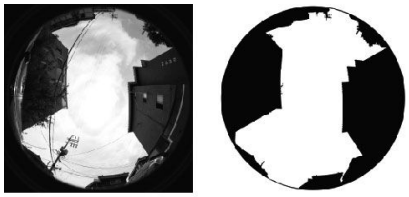

SVF=0.52

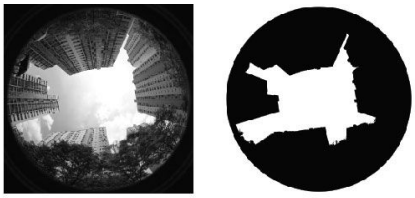

SVF=0.24

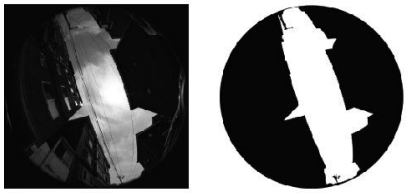

SVF=0.27

SVF=0.40

SVF=0.28

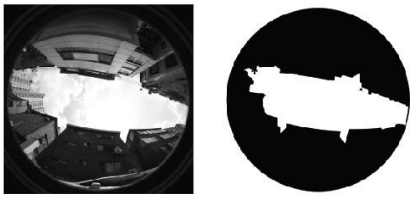

SVF=0.26

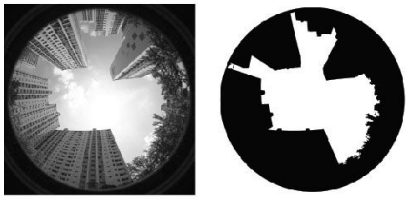

SVF=0.33

SVF=0.40

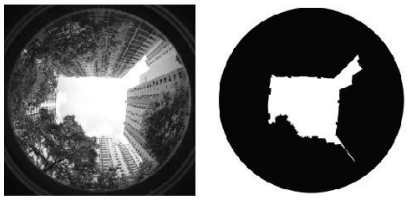

SVF=0.15

SVF=0.46

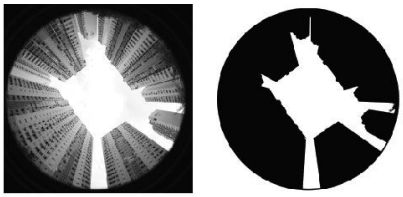

SVF=0.24

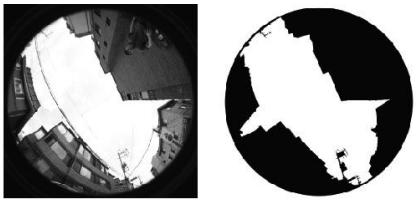

SVF=0.42

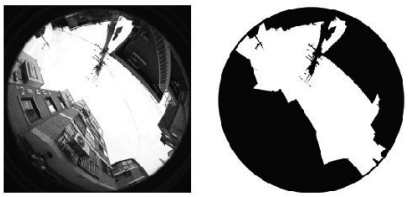

SVF=0.38

SVF=0.37

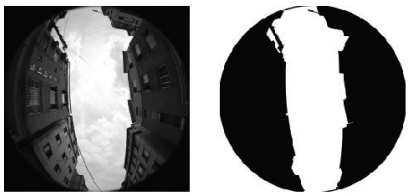

SVF=0.35

■ 국문 초록

서울시 주거지역 옥외공간의 건축형태와 천공률에 따른 주간 표면온도 영향 분석

지도교수 : 이동근
서울대학교 대학원
생태조경·지역시스템공학부(생태조경학)
김준식

도시화 과정에서 가장 뚜렷한 도시기후의 변화는 기온의 상승으로, 이로 인한 도시열섬 현상이 가속화 되었다. 이러한 도시 열섬 현상으로 인해 인간의 건강과 삶의 질에 부정적인 작용들을 초래하고 있다. 이러한 도시열섬을 발생시키는 다양한 원인 중 건축물 조성에 의한 도시의 기하학적 구조(Geometry)의 변화는 건축물 외부공간의 형태, 즉 도시협곡(Urban Canyon) 형태를 변화시키는데, 이로 인해 열환경을 변화를 가져오게 된다. 따라서 도시의 기하학적 구조의 변화에 따른 건축물 외부공간의 열환경 변화를 정량적으로 파악하는 것은, 건축물 조성에 따른 열환경 변화를 파악한다는 점에 있어서 도시계획적 측면에 있어 매우 중요하다.

천공률(Sky view factor;SVF)은 기하학적 구조에 따른 도시협곡을 나타내는 형태를 나타내는 대표 지표로서 건축물의 기하학적 구조뿐만 아니라, 하늘로부터 표면에 받는 라디에이션의 비율을 의미하여 복사평형에 중요 변수로서의 역할을 수행하기 때문에, 도시 구

조와 열환경과의 관계를 분석하기 위한 많은 연구에서 보편적으로 사용되어왔다.

기존의 연구들에서는 천공률을 분석하기 위해 샘플사이트를 선정하여 어안렌즈 사진을 이용한 방법이 일반적으로 사용되었는데 한정된 시간과 한정된 장소에 국한되며, 구름의 양 등이 산정에 영향을 줄 수 있다는 단점이 존재하여 대표성을 띄기 힘들다는 단점이 존재하였었다. 특히 동일한 건축물 사이에서도 산정지점에 따라 천공률이 차이가 존재하는 부분에 대한 반영이 힘들었다는 단점이 존재하였다. 최근에는 이러한 한계를 극복하기 위해 고해상도 지형, 건축물 데이터를 이용하여 시뮬레이션 방식을 통해 천공률을 산정하는 방식의 연구가 상당수 진행되었다. 이 방식은 고해상도의 건축물 데이터와 지형 데이터가 요한다는 단점이 존재하나, 대규모 대상지에 있어서 천공률을 산정하는데 있어서 상세한 천공률을 빠른 시간에 산정할 수 있다는 장점이 존재하며, 효율성이 높기 때문에 최근의 연구에서 사용빈도가 높아지고 있다.

또한 열환경을 파악하기 위해 온도값을 취득하는데 있어서 기존 연구들에서는 천공률과 마찬가지로 샘플 사이트에 대한 측정을 통해 공기온도 값을 취득하는 방식으로 주로 연구가 되어왔다. 그러나 다양한 변수들에 의해 영향을 받는 미기후 특성상 충분한 샘플 없이 대표성을 띄기 힘들다는 한계점을 지녔었다. 따라서 대규모 대상지에 있어서 동시간의 온도값을 취득하여 상대적 열분포 파악에 유리한 위성영상을 이용한 지표면온도 산정 방식은 많은 연구에서 사용되고 있다.

이러한 장점으로 인해 최근에는 시뮬레이션된 천공률과 위성영상을 이용해 산정한 지표면온도를 이용하여 열환경을 평가하고자 한

연구 등이 Scarano and Sobrino(2015) 등을 통해 수행되었으나, 한계점들이 존재하였다. 첫째로, 용도지역에 따라 다른 패턴을 나타내는 지표면온도의 특성에 대한 고려가 부족하였으며, 두 번째로 Landsat 8의 특성상 30m 간격으로 값이 추출되기 때문에, 건축물 외부지역의 천공률을 파악하기 위해서는 지붕 비율(건폐율)의 통제에 따른 지표면온도의 영향이 고려되어야 하나 이에 대한 고려가 이루어지지 못하였다. 세 번째로 녹지, 강, 하천 등의 냉섬 효과에 대한 입지적 특성 고려 및 토지피복 특성에 대한 통제가 필요하나 이에 대한 고려가 이루어지지 못하였다는 한계점이 존재하였다. 또한 대상지의 건축 특성상 빌딩의 배치 등을 고려한 영향을 파악하는 수준에는 이르지 못하였다.

본 연구는 이러한 중요성, 기존연구의 한계를 바탕으로 건축물의 형태에 따라 생성되는 건축물 외부 공간, 이로 인해 발생되는 열환경의 변화를 파악하고자 하였다. 따라서 시뮬레이션을 통해 구축한 서울시의 천공률과 Landsat 8 위성 영상을 통해 구축한 지표면온도(Land Surface Temperature;LST)를 이용하여, 지붕비율(건폐율) 별 건축물의 높이, 천공률, 지표면온도 간의 유기적인 관계에 관한 분석하고, 이에 대한 결과의 원인에 대해서 선행연구를 통한 기작 분석과 단지 내 녹지 분석을 통해 파악하고자 하였다. 특히 노인과 어린이 등이 열환경에 노출되기 쉬운 주거지역으로 용도지역을 제한하여 주거지역의 건축물에 의한 열환경을 파악하고자 하였다. 이에 있어 한강, 하천, 산, 대녹지 등의 열저감원의 직접 영향을 통제하고, 지표면온도의 공간적 해상도를 한계를 고려하여 유사 지붕비율(건폐율)간의 비교를 통해 건축물 높이, 건축물 외부공간의 천공률, 건축물 외부 공간의 지표면온도 간의 유기적인 관계를 파악하고자 하였다.

본 연구의 결과를 요약하면 첫째, 높이가 낮은 단독, 다가구, 다세대 주택들은 건축물 외부의 도시협곡의 형태에 있어서 높은 천공률을 생성하며, 이로 인한 직달일사량 증가에 의해 지표면의 순복사량이 상승하여 건축물 외부공간의 주간 지표면온도가 상대적으로 높게 나타난 것으로 파악되었다. 반면에 높이가 높은 판상형, 탑상형 아파트들은 낮은 천공률의 건축물 외부공간을 생성하여 상대적으로 건축물 외부공간의 주간 지표면온도가 낮음을 파악할 수 있었다.

둘째, 고층 건축물에 있어서 같은 높이일지라도 다른 천공률 값을 갖는 경우가 존재하였는데, 이러한 현상은 고층의 판상형 아파트 배치에 의한 것으로 파악할 수 있었다. 실제로 구축된 천공률 데이터를 기반으로 0.2 이하 값을 추출해 파악해본 결과, 판상형 아파트 단지 내에서도 개방된 'L'자, 'I'자 구조의 경우 천공률 0.2 이하의 값이 많이 도출되지 않는 것을 파악할 수 있었다. 반면 판상형 아파트의 'C'자, 'O'자 등의 폐쇄된 배치는 천공률 0.2 이하의 값을 다수 추출하는 것으로 나타났다. 또한 이러한 지역의 주간 지표면온도는 오히려 천공률이 낮아질수록 다소 상승하는 것을 파악할 수 있었다. 이렇듯 판상형 아파트가 폐쇄된 배치를 취하는 지역의 경우 주간 지표면온도가 높으며, 야간의 경우 복사냉각 저하로 인해 열대야 현상이 더욱 가속화 될 것으로 판단되는 바, 폐쇄형 배치를 지양해야 한다고 판단되었다.

이러한 결과에 대해서 천공률 0.2 이하 구간에 주목하여 원인을 파악하기 위해 선행연구를 파악하여 원인을 분석한 결과, 두 가지의 가설로서 이러한 현상의 원인을 밝히고자 하였다. 첫 번째 가설은, 천공률이 낮은 구간에서 야간의 장파복사저하로 인한 반복사의 증가로 복사냉각이 저하되어 지표면온도가 덜 감소하는 현상이 발생

하는데 이러한 충분하게 냉각되지 않은 표면의 영향이 주간(11시)까지 영향을 미쳤다는 점을 유추할 수 있었다. 이는 영상이 촬영된 11시의 경우, 매우 낮은 SVF 값을 갖는 경우에 직달일사량이 지면까지 충분하게 투입되지 않았기 때문에 야간의 패턴이 유지되는 것으로 판단되었다.

두 번째 가설로서 천공률 0.2 이하 구간의 경우 해당 지역의 녹지의 부족으로 인해 이러한 현상이 발생하였다고 설정하였다. 실제로 문수영(2011)의 연구에서와 같이 천공률이 낮은 형태인 판상형 아파트가 폐쇄된 형태로 배치될 때 주차장으로 사용하는 경우가 많으며, 상대적으로 녹지량이 적은 특징을 지님을 확인할 수 있었다. 따라서 천공률에 따른 녹지를 대표하는 NDVI 값을 파악하여 이상구간의 원인을 파악해본 결 과 모든 구간에서 천공률이 상승할수록 NDVI가 상승하는 정적인 관계를 나타냄을 파악할 수 있었고, 특히 천공률 값이 0-0.2의 구간의 경우 천공률 상승에 따라 상대적으로 큰폭의 NDVI 값 상승이 나타났다. 따라서 이러한 피복 차이에 의해 지표면 온도가 영향을 받았음을 파악할 수 있었다. 구간별로 살펴보면 천공률 값이 0.2 이하의 구간에서는 천공률이 상승할 때 NDVI가 상승하고, 지표면온도 값이 다소 낮아지는 패턴을 통해, NDVI 증가가 지표면 온도 저감에 영향을 미침을 파악할 수 있었다. 천공률 값이 0.2 이상의 구간에서는 녹지량이 증가함에도 불구하고 지표면온도 값이 상승하는 것을 통해 지면에 도달하는 직달일사량이 급격한 증가로 인해 상승한 것으로 파악하였다.

본 연구는 고해상도 시뮬레이션을 통한 천공률과 위성영상을 통한 지표면온도를 이용하여 주거지역의 건축물의 형태, 건축물의 외부공간, 열환경 간의 유기적인 관계를 파악했다는 점에 의의를 지닌

다. 본 연구의 결과는 도시설계의 기초자료로 사용될 수 있을 것이라 판단되며, 궁극적으로는 지속가능한 개발에 기여할 수 있을 것이라고 생각된다.

❑ *주요어 : 천공률, 지표면온도, 건축물 높이, NDVI, Landsat 8, 주거지역, 도시열섬*

❑ *학 번 : 2014-22917*